# Construction of Soliton Solutions of Time-Fractional Caudrey–Dodd–Gibbon–Sawada–Kotera Equation with Painlevé Analysis in Plasma Physics

Khadija Shakeel [1], Alina Alb Lupas [2,*], Muhammad Abbas [1], Pshtiwan Othman Mohammed [3,4,*], Farah Aini Abdullah [5] and Mohamed Abdelwahed [6]

[1] Department of Mathematics, University of Sargodha, Sargodha 40100, Pakistan
[2] Department of Mathematics and Computer Science, University of Oradea, 410087 Oradea, Romania
[3] Department of Mathematics, College of Education, University of Sulaimani, Sulaymaniyah 46001, Iraq
[4] Research and Development Center, University of Sulaimani, Sulaymaniyah 46001, Iraq
[5] School of Mathematical Sciences, Universiti Sains Malaysia, Penang 11800, Malaysia
[6] Department of Mathematics, College of Science, King Saud University, P.O. Box 2455, Riyadh 11451, Saudi Arabia
* Correspondence: dalb@uoradea.ro (A.A.L.); pshtiwansangawi@gmail.com (P.O.M.)

**Abstract:** Fractional calculus with symmetric kernels is a fast-growing field of mathematics with many applications in all branches of science and engineering, notably electromagnetic, biology, optics, viscoelasticity, fluid mechanics, electrochemistry, and signals processing. With the use of the Sardar sub-equation and the Bernoulli sub-ODE methods, new trigonometric and hyperbolic solutions to the time-fractional Caudrey–Dodd–Gibbon–Sawada–Kotera equation have been constructed in this paper. Notably, the definition of our fractional derivative is based on the Jumarie's modified Riemann–Liouville derivative, which offers a strong basis for our mathematical explorations. This equation is widely utilized to report a variety of fascinating physical events in the domains of classical mechanics, plasma physics, fluid dynamics, heat transfer, and acoustics. It is presumed that the acquired outcomes have not been documented in earlier research. Numerous standard wave profiles, such as kink, smooth bell-shaped and anti-bell-shaped soliton, W-shaped, M-shaped, multi-wave, periodic, bright singular and dark singular soliton, and combined dark and bright soliton, are illustrated in order to thoroughly analyze the wave nature of the solutions. Painlevé analysis of the proposed study is also part of this work. To illustrate how the fractional derivative affects the precise solutions of the equation via 2D and 3D plots.

**Keywords:** Caudrey–Dodd–Gibbon–Sawada–Kotera equation; Bernoulli Sub-ODE method; Sardar sub-equation method; Jumarie's modified Riemann–Liouville derivative; soliton solutions; Painlevé Analysis

**MSC:** 35C08; 35C09; 35Q51

## 1. Introduction

The fractional calculus (FC) [1] is an adaptation of classical calculus that is extended to include non-integer (fractional) order integration and differentiation operations. The introduction of the notion of fractional operators occurred nearly concurrently with the advancement of the classical ones. The first recorded mention of the semi-derivative is in a 1695 conversation between a German and French mathematician, namely Gotfield William Leibniz and Guillaume François Antoine, Marquis de l'Hôpital, wherein the meaning of the term is questioned [2]. As a result, many eminent mathematicians, including Riemann, Grünwald, Liouville, Letnikov, Laplace, Euler, and many more, were interested in this topic. The theory of FC has advanced quickly since the 19th century, primarily serving as a

basis for several applied fields such as fractional geometry, fractional differential equations (FDE), and fractional dynamics [3–5]. The study of FC and its numerous applications in the fields of engineering, physical science, and life sciences have received a lot of attention over the past three decades. Numerous fields can be successfully deprived by linear or nonlinear fractional order differential equations, including chemical physics, optics, electrical networks, solitary waves, control theory of dynamical systems, probability and statistics, electrochemistry of corrosion and signal processing, and so forth, and also use FC [6–8].

It is commonly known that nonlinear partial differential equations (NLPDEs) [9] are a useful tool for modeling complicated events in a wide range of scientific domains, including mathematical physics, biology, applied mathematics, chemical physics, optical science, engineering, and so forth. NLPDEs also find extensive use in several domains such as solid state physics, fluid mechanics, neuro physics, mathematical biology, quantum field theory, optical fibers, and plasma physics [10–13]. Innumerable useful domains, including oceanography, meteorology, and the aerospace industry, mostly rely on an understanding of these NLPDEs [14–17]. Several scholars are interested in the efficient ways to develop analytical solutions to nonlinear issues.

The term "soliton" [18,19] refers to a a very stable, nonlinear, self-reinforcing localized wave packet that retains its shape even after interacting with other similar localized wave packets and spreads freely at a constant speed and is widely used in fractional dynamics, engineering finance, physics, and biology. For some classes of NLPDEs, solitons are interesting solutions that propagate with their form and velocity intact without variance. By using analytical approaches such as the tanh-coth method [20], unified transform method [21], rational-expansion technique [22], modified F-expansion method [23], novel Kudryashov approach [24], Hirota's technique [25], bilinear approach [26], modified Khater method [27], direct algebraic method [28], and generalized Khater method [29], a broad category for finding analytical solutions of various NLPDEs such as the following: the Chen–Lee–Liu (CLL) equation [30], the Kadomtsev–Petviashvili equation [31], Mikhailov–Novikov–Wang equation [32], tsunami waves [33], the modified equal width equation [34], the fractional biological population (FBP) model [35], the ill-posed Boussinesq (IPB) equation [36], the Monge Ampere equation [37], and the Davey–Stewartson equation [38], to obtain the appropriate solitons solutions.

A variety of definitions pertaining to the importance of the fractional order derivative have been explored: the Katugampola derivative [39], the Sonin–Letnikov derivative [40], the Grunwald–Letnikov derivative [41], the Davidson derivative [42], the $\beta$-derivative [43], the M-truncated derivative (M-TD) [44], the conformable derivative (C-D) [45], and the Atangana–Baleanu derivative [46] under the context of Caputo. The principal focus of this investigation has been the analysis of effective solutions using the fractional derivative, or the modified Riemann–Liouville derivative (RLD) [47,48], in accordance with the Caudrey–Dodd–Gibbon–Sawada–Kotera model [49,50].

The limitations emerged regarding the generally acknowledged Riemann–Liouville [51] definition of fractional derivatives, which does not enable the derivative of a constant to be zero. The most beneficial solution that has been recommended for tackling this element is the so-called Caputo derivative [52], but employing it subjects us to the unpleasant condition that, in the extreme case, we need to have the function's second derivative in order to acquire the derivative of the function. Alternatively, with this scheme, fractional derivative is only applied to differentiable functions. To cope with this problem, in 2006, Jumarie suggested an alteration of the RLD, modified RLD [47], for tackling non-differentiable functions. This adjustment claims to offer a framework for a fractional calculus that bears substantial parallels to classical calculus.

One of the fundamental models of soliton theory is the fifth-order nonlinear evolution equation. It is referred to in the literature as the Sawada–Kotera (SK) equation or the Caudrey–Dodd–Gibbon–Sawada–Kotera (CDGSK) [49,50] equation because it was proposed more than 40 years ago by Sawada and Kotera as well as independently by Caudrey,

Dodd, and Gibbon. Many approaches have been used in the many publications that have already been published to study the fifth-order CDGSK equation such as Lie symmetry analysis [53], the extended Kudryashov's method [54], the Hirota bilinear method ensuing one soliton, two soliton, and three soliton solutions [55], the new auxiliary equation method resulting in bell, anti-bell, periodic, and singular wave solutions [49], the Bernoulli sub-equation function approach ensuing bright, dark, and oscillating solutions [50], and the integrability of the equation is ascertained by Painlevé analysis [56]. The CDGSK hierarchy's explicit Riemann theta function representations are built employing the theory of Riemann surfaces [57]. A number of integrable features are also derived for the CDGSK problem in addition to the soliton solutions, including the Bäcklund transformation, the Lax pair, and the nonlinear superposition formula [58]. Also, the Bäcklund and Darboux transformations were employed in bilinear forms to evaluate the CDGSK problem.

In this paper, we will precisely solve the time-fractional CDGSK equation [49,50]. We utilize the modified RLD [47,48] by Jumarie as a fractional derivative. For analytical solutions, the CDGSK equation [49] is taken to be as follows:

$$\wp_\tau + \wp_{\chi\chi\chi\chi\chi} + (60\wp^3 + 30\wp\wp_{\chi\chi})_\chi = 0. \tag{1}$$

The structure of the proposed model in the fractional modified RLD derivative is as follows:

$$D_\tau^\kappa \wp + \wp_{\chi\chi\chi\chi\chi} + 30\wp\wp_{\chi\chi\chi} + 30\wp_\chi\wp_{\chi\chi} + 180\wp^2\wp_\chi = 0. \tag{2}$$

where $D_t^\kappa$ is a fractional modified RLD derivative.

Two distinct strategies are applied in order to acquire the required solutions: the Bernoulli sub-ODE method (BSOM) [59] and the Sardar sub-equation technique (SSET) [60]. These techniques are easy to apply and uncomplicated. Our model was not previously implemented with these methods.

The article is formatted in the following way: Section 2 provides definitions of fractional derivatives and an explanation of their properties. In Section 3, the fractional CDGSK equation is mathematically analyzed. In Section 4, the description of analytical techniques is given. In Section 5, the suggested model is subjected to the BSOM method and the SSET analytical steps. In Section 6, computations and graphs are used to show how the outcomes can be explained physically and in Section 7, comparisons of the results are done. Section 8 provides the Painlevé analysis and Section 9 concludes the study with a few closing remarks.

## 2. Preliminaries

In this section, the definitions of fractional derivative and its basic characteristics are covered.

*The Jumarie's Modified Riemann–Liouville Derivative*

**Definition 1.** *The Jumarie's modified Riemann–Liouville derivative [50] of order $\kappa$ is defined by the following:*

$$D_t^\kappa \wp(t) = \begin{cases} \frac{1}{\Gamma(1-\kappa)} \int\limits_0^t (t-\varphi)^{-\kappa-1}(\wp(\varphi) - \wp(0))d\varphi, & \kappa < 0 \\ \frac{1}{\Gamma(1-\kappa)} \frac{d}{dt} \int\limits_0^t (t-\varphi)^{-\kappa}(\wp(\varphi) - \wp(0))d\varphi, & 0 < \kappa < 1 \\ \left(\wp^{(n)}(t)\right)^{\kappa-n}, & n \leq \kappa < n+1, n \geq 1. \end{cases}$$

*The Jumarie's modified Riemann–Liouville derivative has the following properties.*

1. $D_t^\kappa \psi^N = \frac{\Gamma(N+1)}{\Gamma(N+1-\kappa)} \psi^{N-\kappa}, N > 0.$
2. $D_t^\kappa \ell = 0, \quad \ell$ *is a constant.*
3. $D_t^\kappa(\ell_1 r(t) + \ell_2 s(t)) = \ell_1 D_t^\kappa r(t) + \ell_2 D_t^\kappa s(t), \quad \ell_1$ *and* $\ell_2$ *are constants.*

4. $\quad D_t^\kappa(r(t)s(t)) = s(t)D_t^\kappa r(t) + r(t)D_t^\kappa s(t).$
5. $\quad D_t^\kappa r(s(t)) = r'_s[s(t)]D_t^\kappa s(t) = D_t^\kappa r[s(t)](s'(t))^\kappa.$

## 3. Mathematical Analysis of the Procedure

The time-fractional CDGSK equation's (1) wave equation is produced using the subsequent wave transformation

$$\wp(\chi, \tau) = \wp(\varphi), \tag{3}$$

$$\varphi = \hbar_1 \chi - \frac{\hbar_2 \tau^\alpha}{\Gamma(1 + \alpha)}, \tag{4}$$

where $\hbar_1$ and $\hbar_2$ are nonzero arbitrary constants. Equation (4) and Equation (3)'s transformations are employed to generate Equation (2):

$$-\hbar_1\hbar_2\wp' + (\hbar_1^5\wp'''' + 30\hbar_1^3\wp\wp'' + 60\hbar_1\wp^3)' = 0, \tag{5}$$

where $\wp' = \frac{d\wp}{d\varphi}$. Integrating the Equation (5) with zero integration constants, we have

$$-\hbar_1\hbar_2\wp + \hbar_1^5\wp'''' + 30\hbar_1^3\wp\wp'' + 60\hbar_1\wp^3 = 0. \tag{6}$$

## 4. Description of Analytical Methods

### 4.1. Bernoulli Sub-ODE Method

This section explains how to get the traveling wave solutions of NLPDEs using the BSOM [59]. Assume that the partial differential equation for a nonlinear system, with two independent variables, $\chi$ and $t$, is as follows:

$$R(\wp, \wp_\tau, \wp_\chi, \wp_{\tau\tau}, \wp_{\chi\chi}, \wp_{\chi\tau}, \ldots \ldots \ldots) = 0, \tag{7}$$

where $R$ is a polynomial of $\wp(\chi, \tau)$ and its partial derivatives, which involve the highest order derivatives and nonlinear terms, and $\wp(\varphi) = \wp(\chi, \tau)$ is an unknown function. The key steps of this procedure are listed below.

- Step 1: With the independent variables $\chi$ and $\tau$ combined into a single variable $\varphi = \chi \pm \mu\tau$, we assume that

$$\wp(\varphi) = \wp(\chi, \tau), \quad \varphi = \chi \pm \mu\tau. \tag{8}$$

The transformation provided in Equation (8) allows Equation (7) to be changed to the following ODE:

$$R(\wp, \wp', \wp'', \ldots \ldots \ldots) = 0, \tag{9}$$

where $\wp'(\varphi) = \frac{d\wp}{d\varphi}$ and $R$ is a polynomial in $\wp(\varphi)$ and its derivatives.

- Step 2: We assume that the formal solution to Equation (9) exists:

$$\wp(\varphi) = \sum_{i=0}^{k} g_i\Re^i, \quad g_i \neq 0, \tag{10}$$

where $\Re = \Re(\varphi)$ satisfy the equation,

$$\Re' + \psi\Re = \zeta\Re^2, \tag{11}$$

and $g_i(-k \leq i \leq k; k \in N)$ are constants to be determined later, and $\psi \neq 0$.
when $\zeta \neq 0$, Equation (11) is the type of Bernoulli equation, we can obtain the solution as

$$\Re = \frac{\psi}{\zeta + \psi C \exp(\psi\varphi)}, \tag{12}$$

where $C$ is an arbitrary constant.

When $\zeta = 0$, Equation (12) reduces to

$$\Re = \frac{1}{C} \exp(-\psi \varphi). \tag{13}$$

Setting $C = \frac{\zeta}{\psi}$ in Equation (12), we obtain

$$\Re = -\frac{\psi}{2\zeta} \left( \tanh\left( \frac{\psi}{2} \varphi \right) - 1 \right). \tag{14}$$

Setting $C = -\frac{\zeta}{\psi}$ in Equation (12), we obtain

$$\Re = -\frac{\psi}{2\zeta} \left( \coth\left( \frac{\psi}{2} \varphi \right) - 1 \right). \tag{15}$$

- Step 3: Taking into account the homogenous balance between the highest order derivatives and the nonlinear terms found in Equation (7) or (9), one can ascertain the positive integer $k$. Additionally, we precisely define the degree of $\wp(\varphi)$ as $D(\wp(\varphi)) = k$, which in turn yields the degree of the following other expressions:

$$D\left( \frac{d^n \wp}{d\varphi^n} \right) = k + n, \quad D\left( \wp^p \left( \frac{d^n \wp}{d\varphi^n} \right)^s \right) = kp + s(k + n). \tag{16}$$

  Consequently, we can use Equation (16) to determine the value of $k$ in Equation (10).
- Step 4: A system of algebraic Equations is produced by substituting Equation (10) into Equation (9) using Equation (11), gathering all terms of the same powers of $\Re(\varphi)$ together, and setting each coefficient of them to zero. We find the values of $\nu_i$ and $\mu$ by solving this system. Lastly, we derive the exact traveling wave solutions of Equation (7) by inserting $\nu_i$, $\mu$, and Equations (14) and (15) into Equation (10).

*4.2. Sardar Sub-Equation Technique*

We will address an NLPDE in its general form as follows:

**Step 1:**

$$R(N, N_\tau, N_\chi, N_{\tau\tau}, N_{\chi\chi}, N_{\chi\tau}, \ldots \ldots \ldots) = 0, \tag{17}$$

in which $\wp(\varphi) = \wp(\chi, \tau)$ is an unknown function and $R$ is a polynomial of $\wp$. Consider the wave transformation,

$$\varphi = \eta\chi + \mu\tau, \tag{18}$$

in which $\eta$ and $\mu$ are non-zero real constants. The transformation is used to change Equation (17) into the subsequent ODE.

$$R(N, N', N'', \ldots \ldots \ldots) = 0 \tag{19}$$

where $R$ is a polynomial in $\wp$ and the ordinary derivatives of $R$ are represented by the superscripts pertaining to $\varphi$.

**Step 2:** Let us assume that the NLPDE in Equation (7) has the following solution:

$$N(\varphi) = \sum_{i=0}^{k} r_i \Im(\varphi)^i, \quad r_i \neq 0, \tag{20}$$

where $r_k(0 \leq k \leq N)$ are real constants and $\Im(\varphi)$ satisfying the ode in the form

$$\Im'(\varphi) = \sqrt{f + u\Im(\varphi)^2 + \Im(\varphi)^4}, \tag{21}$$

where $f$ and $u$ are real constants and Equation (21) presents the solutions as follows:

**Case I:** if $u > 0$ and $f = 0$, then

$$\Im_1^{\pm}(\varphi) = \pm\sqrt{-lmu}\,\operatorname{sech}_{lm}\left(\sqrt{u}\varphi\right),$$

$$\Im_2^{\pm}(\varphi) = \pm\sqrt{lmu}\,\operatorname{csch}_{lm}\left(\sqrt{u}\varphi\right),$$

where

$$\operatorname{sech}_{lm}(\varphi) = \frac{2}{le^{\varphi} + me^{-\varphi}}, \quad \operatorname{csch}_{lm}(\varphi) = \frac{2}{le^{\varphi} - me^{-\varphi}}, \quad \textit{where } l, m \textit{ are non zero real values.}$$

**Case II:** if $u < 0$ and $f = 0$, then

$$\Im_3^{\pm}(\varphi) = \pm\sqrt{-lmu}\,\sec_{lm}\left(\sqrt{-u}\varphi\right),$$

$$\Im_4^{\pm}(\varphi) = \pm\sqrt{-lmu}\,\csc_{lm}\left(\sqrt{-u}\varphi\right),$$

where

$$\sec_{lm}(\varphi) = \frac{2}{le^{\iota\varphi} + me^{-\iota\varphi}}, \quad \csc_{lm}(\varphi) = \frac{2\iota}{le^{\iota\varphi} - me^{-\iota\varphi}}, \quad \textit{where } l, m \textit{ are non zero real values.}$$

**Case III:** if $u < 0$ and $f = \frac{u^2}{4}$, then

$$\Im_5^{\pm}(\varphi) = \pm\sqrt{\frac{-u}{2}}\,\tanh_{lm}\left(\sqrt{\frac{-u}{2}}\varphi\right),$$

$$\Im_6^{\pm}(\varphi) = \pm\sqrt{\frac{-u}{2}}\,\coth_{lm}\left(\sqrt{\frac{-u}{2}}\varphi\right),$$

$$\Im_7^{\pm}(\varphi) = \pm\sqrt{\frac{-u}{2}}\left(\tanh_{lm}(\sqrt{-2u}\varphi) \pm \iota\sqrt{lm}\,\operatorname{sech}_{lm}\left(\sqrt{-2u}\varphi\right)\right),$$

$$\Im_8^{\pm}(\varphi) = \pm\sqrt{\frac{-u}{2}}\left(\coth_{lm}(\sqrt{-2u}\varphi) \pm \iota\sqrt{lm}\,\operatorname{csch}_{lm}\left(\sqrt{-2u}\varphi\right)\right),$$

$$\Im_9^{\pm}(\varphi) = \pm\sqrt{\frac{-u}{8}}\left(\tanh_{lm}(\sqrt{\frac{-u}{8}}\varphi) + \coth_{lm}\left(\sqrt{\frac{-u}{8}}\varphi\right)\right),$$

where

$$\tanh_{lm}(\varphi) = \frac{le^{\varphi} - me^{-\varphi}}{le^{\varphi} + me^{-\varphi}}, \quad \coth_{lm}(\varphi) = \frac{le^{\varphi} + me^{-\varphi}}{le^{\varphi} - me^{-\varphi}}, \quad \textit{where } l, m \textit{ are non zero real values.}$$

**Case IV:** if $u > 0$ and $f = \frac{u^2}{4}$, then

$$\Im_{10}^{\pm}(\varphi) = \pm\sqrt{\frac{u}{2}}\,\tan_{lm}\left(\sqrt{\frac{u}{2}}\varphi\right),$$

$$\Im_{11}^{\pm}(\varphi) = \pm\sqrt{\frac{u}{2}}\,\cot_{lm}\left(\sqrt{\frac{u}{2}}\varphi\right),$$

$$\Im_{12}^{\pm}(\varphi) = \pm\sqrt{\frac{u}{2}}\left(\tan_{lm}\left(\sqrt{2u}\varphi\right) \pm \sqrt{lm}\,\sec_{lm}\left(\sqrt{2u}\varphi\right)\right),$$

$$\Im_{13}^{\pm}(\varphi) = \pm\sqrt{\frac{u}{2}}\left(\cot_{lm}\left(\sqrt{2u}\varphi\right) \pm \sqrt{lm}\,\csc_{lm}\left(\sqrt{2u}\varphi\right)\right),$$

$$\Im_{14}^{\pm}(\varphi) = \pm\sqrt{\frac{u}{8}}\left(\tan_{lm}\left(\sqrt{\frac{u}{8}}\varphi\right) + \cot_{lm}\left(\sqrt{\frac{u}{8}}\varphi\right)\right),$$

where

$$\tan_{lm}(\varphi) = -\iota\frac{le^{\iota\varphi} - me^{-\iota\varphi}}{le^{\iota\varphi} + me^{-\iota\varphi}}, \quad \cot_{lm}(\varphi) = \iota\frac{le^{\iota\varphi} + me^{-\iota\varphi}}{le^{\iota\varphi} - me^{-\iota\varphi}}, \quad \text{where } l, m \text{ are non zero real values.}$$

These functions, with non-zero parameters $l$ and $m$, are generalized hyperbolic and trigonometric functions. They emerge as hyperbolic and trigonometric functions if we assign $l = m = 1$.

**Step 3:** Using the homogeneous balancing rule, we begin the process by determining $k$. Once k has been determined, insert Equations (20) and (21) into Equation (19). All of the powers of $\Im(\varphi)$ must have their coefficients equal to zero since we are searching for a non-zero solution to $\Im(\varphi) = 0$.

**Step 4:** The necessary parameters and the precise solution to the given equation can be found using this set of Equations.

## 5. Application of Analytical Techniques

### 5.1. Bernoulli Sub-ODE Method

We determine the value of $k$ by applying a homogeneous balancing principle to Equation (6), which yields $k = 2$. So Equation (10) becomes

$$\wp(\varphi) = g_0 + g_1\Re(\varphi) + g_2\Re(\varphi)^2, \tag{22}$$

where the constants $g_0, g_1, g_2$ are variables that can be found later. Plugging Equation (22) and (11) into Equation (6) yields

$$
\begin{aligned}
&-\hbar_1\hbar_2 g_0 + 60\hbar_1 g_0^3 - \hbar_1\hbar_2 g_1\wp(\varphi) + \psi^4\hbar_1^5 g_1\wp(\varphi) - 15\psi^3\zeta\hbar_1^5 g_1\wp(\varphi)^2 + 50\psi^2\zeta^2\hbar_1^5 g_1\wp(\varphi)^3 - 60\psi\zeta^3\hbar_1^5 g_1\wp(\varphi)^4 \\
&24\zeta^4\hbar_1^5 g_1\wp(\varphi) + 30\psi^2\hbar_1^3 g_1 g_0\wp(\varphi) - 90\psi\zeta\hbar_1^3 g_1 g_0\wp(\varphi)^2 + 60\zeta^2\hbar_1^3 g_1 g_0\wp(\varphi)^3 + 180\hbar_1 g_0^2 g_1\wp(\varphi) + 30\psi^2\hbar_1^3 g_1^2\wp(\varphi)^2 \\
&- 90\psi\zeta\hbar_1^3 g_1^2\wp(\varphi)^3 + 60\zeta^2\hbar_1^3 g_1^2\wp(\varphi)^4 + 180\hbar_1 g_0 g_1^2\wp(\varphi)^2 + 60\hbar_1 g_1^3\wp(\varphi)^3 - \hbar_1\hbar_2 g_2\wp(\varphi)^2 + 16\psi^4\hbar_1^5 g_2\wp(\varphi)^2 - \\
&130\psi^3\zeta\hbar_1^5 g_2\wp(\varphi)^3 + 330\psi^2\zeta^2\hbar_1^5 g_2\wp(\varphi)^4 - 336\psi\zeta^3\hbar_1^5 g_2\wp(\varphi)^5 + 120\zeta^4\hbar_1^5 g_2\wp(\varphi)^6 + 120\psi^2\hbar_1^3 g_0 g_2\wp(\varphi)^2 - \\
&300\psi\zeta\hbar_1^3 g_0 g_2\wp(\varphi)^3 + 180\zeta^2\hbar_1^3 g_0 g_2\wp(\varphi)^4 + 180\hbar_1 g_0^2 g_2\wp(\varphi)^2 + 150\psi^2\hbar_1^3 g_1 g_2\wp(\varphi)^3 - 390\psi\zeta\hbar_1^3 g_1 g_2\wp(\varphi)^4 + \\
&240\zeta^2\hbar_1^3 g_1 g_2\wp(\varphi)^5 + 360\hbar_1 g_0 g_1 g_2\wp(\varphi)^3 + 180\hbar_1 g_1^2 g_2\wp(\varphi)^4 + 120\psi^2\hbar_1^3 g_2^2\wp(\varphi)^4 - 300\psi\zeta\hbar_1^3 g_2^2\wp(\varphi)^5 + \\
&180\zeta^2\hbar_1^3 g_2^2\wp(\varphi)^6 + 180\hbar_1 g_0 g_2^2\wp(\varphi)^4 + 180\hbar_1 g_1 g_2^2\wp(\varphi)^5 + 60\hbar_1 g_2^3\wp(\varphi)^6 = 0. \tag{23}
\end{aligned}
$$

Equating each coefficient of $\wp(\varphi)^p$ to zero, where ($p = 0, 1, 2, 3, 4, 5$ and $6$), we have

$$
\begin{aligned}
\wp(\varphi)^0 &: -\hbar_2\hbar_1 g_0 + 60\hbar_1 g_0^3 = 0, \\
\wp(\varphi)^1 &: -\hbar_1\hbar_2 g_1 + \psi^4\hbar_1^5 g_1 + 30\psi^2\hbar_1^3 g_0 g_1 + 180\hbar_1 g_0^2 g_1 = 0, \\
\wp(\varphi)^2 &: -15\psi^3\zeta\hbar_1^5 g_1 - 90\psi\zeta\hbar_1^3 g_0 g_1 + 30\psi^2\hbar_1^3 g_1^2 + 180\hbar_1 g_0 g_1^2 - \hbar_1\hbar_2 g_2 + 16\psi^4\hbar_1^5 g_2 + 120\psi^2\hbar_1^3 g_0 g_2 + 180\hbar_1 g_0^2 g_2 = 0, \\
\wp(\varphi)^3 &: 50\psi^2\zeta^2\hbar_1^5 g_1 + 60\zeta^2\hbar_1^3 g_0 g_1 - 90\psi\zeta\hbar_1^3 g_1^2 + 60\hbar_1 g_1^3 - 130\psi^3\zeta\hbar_1^5 g_2 - 300\psi\zeta\hbar_1^3 g_0 g_2 + 150\psi^2\hbar_1^2 g_1 g_2 + \\
&\quad 360\hbar_1 g_0 g_1 g_2 = 0, \\
\wp(\varphi)^4 &: -60\psi\zeta^3\hbar_1^5 g_1 + 60\zeta^2\hbar_1^3 g_1^2 + 330\psi^2\zeta^2\hbar_1^5 g_2 + 180\zeta^2\hbar_1^3 g_0 g_2 - 390\psi\zeta\hbar_1^3 g_1 g_2 + 180\hbar_1 g_1^2 g_2 + 120\psi^2\hbar_1^3 g_2^2 + \\
&\quad 180\hbar_1 g_0 g_2^2 = 0, \\
\wp(\varphi)^5 &: 24\zeta^4\hbar_1^5 g_1 - 336\psi\zeta^3\hbar_1^5 g_2 + 240\zeta^2\hbar_1^3 g_1 g_2 - 300\psi\zeta\hbar_1^3 g_2^2 + 180\hbar_1 g_1 g_2^2 = 0, \\
\wp(\varphi)^6 &: 120\zeta^4\hbar_1^5 g_2 + 180\zeta^2\hbar_1^3 g_2^2 + 60\hbar_1 g_2^3 = 0.
\end{aligned}
$$

$$\tag{24}$$

When the aforementioned Equations for $\hbar_1$, $\hbar_2$, $\psi$, $g_0$, $g_1$, and $g_2$ are solved, we obtain

**Case 1.** If $g_0 = \frac{1}{120}\left(-15\psi^2\hbar_1^2 - \sqrt{105}\psi^2\hbar_1^2\right)$, $g_1 = \psi\zeta\hbar_1^2$, $g_2 = -\zeta^2\hbar_1^2$, $\hbar_2 = \frac{1}{8}\left(11\psi^4\hbar_1^4 + \sqrt{105}\psi^4\hbar_1^4\right)$, then the following solutions are obtained.

When $\zeta \neq 0$, using the above coefficients and Equation (12) in Equation (22) yields

$$\wp_{1,1}(\chi,\tau) = \frac{1}{120}\left(-15\psi^2\hbar_1^2 - \sqrt{105}\psi^2\hbar_1^2\right) + \psi\zeta\hbar_1^2\left(\frac{\psi}{\zeta + \psi C\exp(\psi\varphi)}\right) - \zeta^2\hbar_1^2\left(\frac{\psi}{\zeta + \psi C\exp(\psi\varphi)}\right)^2.$$

Using above coefficients and Equation (14) in Equation (22) yields

$$\wp_{1,2}(\chi,\tau) = \frac{1}{120}\left(-15\psi^2\hbar_1^2 - \sqrt{105}\psi^2\hbar_1^2\right) + \psi\zeta\hbar_1^2\left(-\frac{\psi}{2\zeta}\left(\tanh\left(\frac{\psi}{2}\varphi\right) - 1\right)\right) - \zeta^2\hbar_1^2\left(-\frac{\psi}{2\zeta}\left(\tanh\left(\frac{\psi}{2}\varphi\right) - 1\right)\right)^2. \quad (25)$$

Using the above coefficients and Equation (15) in Equation (22) yields

$$\wp_{1,3}(\chi,\tau) = \frac{1}{120}\left(-15\psi^2\hbar_1^2 - \sqrt{105}\psi^2\hbar_1^2\right) + \psi\zeta\hbar_1^2\left(-\frac{\psi}{2\zeta}\left(\coth\left(\frac{\psi}{2}\varphi\right) - 1\right)\right) - \zeta^2\hbar_1^2\left(-\frac{\psi}{2\zeta}\left(\coth\left(\frac{\psi}{2}\varphi\right) - 1\right)\right)^2.$$

**Case 2.** If $g_0 = 0$, $g_1 = \frac{\sqrt{\hbar_2}\zeta}{\psi}$, $g_2 = -\frac{\sqrt{\hbar_2}\zeta^2}{\psi^2}$, $\hbar_1 = \frac{\hbar_2^{1/4}}{\psi}$, then the following solutions are obtained.

When $\zeta \neq 0$, using the above coefficients and Equation (12) in Equation (22) yields

$$\wp_{2,1}(\chi,\tau) = \frac{\sqrt{\hbar_2}\zeta}{\psi}\left(\frac{\psi}{\zeta + \psi C\exp(\psi\varphi)}\right) - \frac{\sqrt{\hbar_2}\zeta^2}{\psi^2}\left(\frac{\psi}{\zeta + \psi C\exp(\psi\varphi)}\right)^2.$$

Using the above coefficients and Equation (14) in Equation (22) yields

$$\wp_{2,2}(\chi,\tau) = \frac{\sqrt{\hbar_2}\zeta}{\psi}\left(-\frac{\psi}{2\zeta}\left(\tanh\left(\frac{\psi}{2}\varphi\right) - 1\right)\right) - \frac{\sqrt{\hbar_2}\zeta^2}{\psi^2}\left(-\frac{\psi}{2\zeta}\left(\tanh\left(\frac{\psi}{2}\varphi\right) - 1\right)\right)^2. \quad (26)$$

Using the above coefficients and Equation (15) in Equation (22) yields

$$\wp_{2,3}(\chi,\tau) = \frac{\sqrt{\hbar_2}\zeta}{\psi}\left(-\frac{\psi}{2\zeta}\left(\coth\left(\frac{\psi}{2}\varphi\right) - 1\right)\right) - \frac{\sqrt{\hbar_2}\zeta^2}{\psi^2}\left(-\frac{\psi}{2\zeta}\left(\coth\left(\frac{\psi}{2}\varphi\right) - 1\right)\right)^2.$$

**Case 3.** If $g_0 = \dfrac{-26\sqrt{2}\hbar_2\sqrt{-\frac{(-11+\sqrt{105})\hbar_2}{\psi^4}}\psi^2 + \sqrt{2}\left(-\frac{(-11+\sqrt{105})\hbar_2}{\psi^4}\right)^{3/2}\psi^6}{240\hbar_2}$, $g_1 = \dfrac{\sqrt{-\frac{(-11+\sqrt{105})\hbar_2}{\psi^4}}\psi\zeta}{\sqrt{2}}$, $g_2 = -\dfrac{\sqrt{-\frac{(-11+\sqrt{105})\hbar_2}{\psi^4}}\zeta^2}{\sqrt{2}}$, $\hbar_1 = -\dfrac{\left(\frac{11\hbar_2}{\psi^4} - \frac{\sqrt{105}\hbar_2}{\psi^4}\right)^{1/4}}{2^{1/4}}$, then the following solutions are obtained.

When $\zeta \neq 0$, using the above coefficients and Equation (12) in Equation (22) yields

$$\wp_{3,1}(\chi,\tau) = \frac{-26\sqrt{2}\hbar_2\sqrt{-\frac{(-11+\sqrt{105})\hbar_2}{\psi^4}}\psi^2 + \sqrt{2}\left(-\frac{(-11+\sqrt{105})\hbar_2}{\psi^4}\right)^{3/2}\psi^6}{240\hbar_2} +$$

$$\frac{\sqrt{-\frac{(-11+\sqrt{105})\hbar_2}{\psi^4}}\psi\zeta}{\sqrt{2}}\left(\frac{\psi}{\zeta + \psi C\exp(\psi\varphi)}\right) - \frac{\sqrt{-\frac{(-11+\sqrt{105})\hbar_2}{\psi^4}}\zeta^2}{\sqrt{2}}\left(\frac{\psi}{\zeta + \psi C\exp(\psi\varphi)}\right)^2.$$

Using the above coefficients and Equation (14) in Equation (22) yields

$$\wp_{3,2}(\chi,\tau) = \frac{-26\sqrt{2}\hbar_2\sqrt{-\frac{(-11+\sqrt{105})\hbar_2}{\psi^4}}\psi^2 + \sqrt{2}\left(-\frac{(-11+\sqrt{105})\hbar_2}{\psi^4}\right)^{3/2}\psi^6}{240\hbar_2} -$$

$$\frac{\sqrt{-\frac{(-11+\sqrt{105})\hbar_2}{\psi^4}}\psi\zeta}{\sqrt{2}}\left(-\frac{\psi}{2\zeta}\left(\tanh\left(\frac{\psi}{2}\varphi\right)-1\right)\right) - \frac{\sqrt{-\frac{(-11+\sqrt{105})\hbar_2}{\psi^4}}\zeta^2}{\sqrt{2}}\left(-\frac{\psi}{2\zeta}\left(\tanh\left(\frac{\psi}{2}\varphi\right)-1\right)\right)^2. \quad (27)$$

Using the above coefficients and Equation (15) in Equation (22) yields

$$\wp_{3,3}(\chi,\tau) = \frac{-26\sqrt{2}\hbar_2\sqrt{-\frac{(-11+\sqrt{105})\hbar_2}{\psi^4}}\psi^2 + \sqrt{2}\left(-\frac{(-11+\sqrt{105})\hbar_2}{\psi^4}\right)^{3/2}\psi^6}{240\hbar_2} -$$

$$\frac{\sqrt{-\frac{(-11+\sqrt{105})\hbar_2}{\psi^4}}\psi\zeta}{\sqrt{2}}\left(-\frac{\psi}{2\zeta}\left(\coth\left(\frac{\psi}{2}\varphi\right)-1\right)\right) + \frac{\sqrt{-\frac{(-11+\sqrt{105})\hbar_2}{\psi^4}}\zeta^2}{\sqrt{2}}\left(-\frac{\psi}{2\zeta}\left(\coth\left(\frac{\psi}{2}\varphi\right)-1\right)\right)^2.$$

**Case 4.** If $g_0 = \dfrac{26\sqrt{2}\hbar_2\sqrt{-\frac{(-11+\sqrt{105})\hbar_2}{\psi^4}}\psi^2 - \sqrt{2}\left(-\frac{(-11+\sqrt{105})\hbar_2}{\psi^4}\right)^{3/2}\psi^6}{240\hbar_2}$, $g_1 = -\dfrac{\sqrt{-\frac{(-11+\sqrt{105})\hbar_2}{\psi^4}}\psi\zeta}{\sqrt{2}}$,

$g_2 = \dfrac{\sqrt{-\frac{(-11+\sqrt{105})\hbar_2}{\psi^4}}\zeta^2}{\sqrt{2}}$, $\hbar_1 = -\dfrac{\iota\left(\frac{11\hbar_2}{\psi^4}-\frac{\sqrt{105}\hbar_2}{\psi^4}\right)^{1/4}}{2^{1/4}}$, then the following solutions are obtained.

When $\zeta \neq 0$, using the above coefficients and Equation (12) in Equation (22) yields

$$\wp_{4,1}(\chi,\tau) = \frac{26\sqrt{2}\hbar_2\sqrt{-\frac{(-11+\sqrt{105})\hbar_2}{\psi^4}}\psi^2 - \sqrt{2}\left(-\frac{(-11+\sqrt{105})\hbar_2}{\psi^4}\right)^{3/2}\psi^6}{240\hbar_2} -$$

$$\frac{\sqrt{-\frac{(-11+\sqrt{105})\hbar_2}{\psi^4}}\psi\zeta}{\sqrt{2}}\left(\frac{\psi}{\zeta + \psi C\exp(\psi\varphi)}\right) - \frac{\sqrt{-\frac{(-11+\sqrt{105})\hbar_2}{\psi^4}}\zeta^2}{\sqrt{2}}\left(\frac{\psi}{\zeta + \psi C\exp(\psi\varphi)}\right)^2.$$

Using the above coefficients and Equation (14) in Equation (22) yields

$$\wp_{4,2}(\chi,\tau) = \frac{26\sqrt{2}\hbar_2\sqrt{-\frac{(-11+\sqrt{105})\hbar_2}{\psi^4}}\psi^2 + \sqrt{2}\left(-\frac{(-11+\sqrt{105})\hbar_2}{\psi^4}\right)^{3/2}\psi^6}{240\hbar_2} -$$

$$\frac{\sqrt{-\frac{(-11+\sqrt{105})\hbar_2}{\psi^4}}\psi\zeta}{\sqrt{2}}\left(-\frac{\psi}{2\zeta}\left(\tanh\left(\frac{\psi}{2}\varphi\right)-1\right)\right) + \frac{\sqrt{-\frac{(-11+\sqrt{105})\hbar_2}{\psi^4}}\zeta^2}{\sqrt{2}}\left(-\frac{\psi}{2\zeta}\left(\tanh\left(\frac{\psi}{2}\varphi\right)-1\right)\right)^2. \quad (28)$$

Using the above coefficients and Equation (15) in Equation (22) yields

$$\wp_{4,3}(\chi,\tau) = \frac{26\sqrt{2}\hbar_2\sqrt{-\frac{(-11+\sqrt{105})\hbar_2}{\psi^4}}\psi^2 + \sqrt{2}\left(-\frac{(-11+\sqrt{105})\hbar_2}{\psi^4}\right)^{3/2}\psi^6}{240\hbar_2} -$$

$$\frac{\sqrt{-\frac{(-11+\sqrt{105})\hbar_2}{\psi^4}}\psi\zeta}{\sqrt{2}}\left(-\frac{\psi}{2\zeta}\left(\coth\left(\frac{\psi}{2}\varphi\right)-1\right)\right) + \frac{\sqrt{-\frac{(-11+\sqrt{105})\hbar_2}{\psi^4}}\zeta^2}{\sqrt{2}}\left(-\frac{\psi}{2\zeta}\left(\coth\left(\frac{\psi}{2}\varphi\right)-1\right)\right)^2.$$

**Case 5.** If $g_0 = \dfrac{26\sqrt{2}\hbar_2\sqrt{-\frac{(-11+\sqrt{105})\hbar_2}{\hbar_1^4}}\hbar_1^2 - \sqrt{2}\left(-\frac{(-11+\sqrt{105})\hbar_2}{\hbar_1^4}\right)^{3/2}\hbar_1^6}{240\hbar_2}$, $g_1 = -\dfrac{i\mu\left(-\frac{(-11+\sqrt{105})\hbar_2}{\hbar_1^4}\right)^{1/4}\hbar_1^2}{2^{1/4}}$,

$g_2 = -\mu^2\hbar_1^2$, $\psi = -\dfrac{i\left(\frac{11\hbar_2}{\hbar_1^4} - \frac{\sqrt{105}\hbar_2}{\hbar_1^4}\right)^{1/4}}{2^{1/4}}$, then the following solutions are obtained.
When $\zeta \neq 0$, using the above coefficients and Equation (12) in Equation (22) yields

$$\wp_{5,1}(\chi,\tau) = \frac{26\sqrt{2}\hbar_2\sqrt{-\frac{(-11+\sqrt{105})\hbar_2}{\hbar_1^4}}\hbar_1^2 - \sqrt{2}\left(-\frac{(-11+\sqrt{105})\hbar_2}{\hbar_1^4}\right)^{3/2}\hbar_1^6}{240\hbar_2} -$$

$$\frac{i\mu\left(-\frac{(-11+\sqrt{105})\hbar_2}{\hbar_1^4}\right)^{1/4}\hbar_1^2}{2^{1/4}}\left(\frac{\psi}{\zeta + \psi C \exp(\psi\varphi)}\right) - \mu^2\hbar_1^2\left(\frac{\psi}{\zeta + \psi C \exp(\psi\varphi)}\right)^2.$$

Using the above coefficients and Equation (14) in Equation (22) yields

$$\wp_{5,2}(\chi,\tau) = \frac{26\sqrt{2}\hbar_2\sqrt{-\frac{(-11+\sqrt{105})\hbar_2}{\hbar_1^4}}\hbar_1^2 - \sqrt{2}\left(-\frac{(-11+\sqrt{105})\hbar_2}{\hbar_1^4}\right)^{3/2}\hbar_1^6}{240\hbar_2} -$$

$$\frac{i\mu\left(-\frac{(-11+\sqrt{105})\hbar_2}{\hbar_1^4}\right)^{1/4}\hbar_1^2}{2^{1/4}}\left(-\frac{\psi}{2\zeta}\left(\tanh\left(\frac{\psi}{2}\varphi\right) - 1\right)\right) - \mu^2\hbar_1^2\left(-\frac{\psi}{2\zeta}\left(\tanh\left(\frac{\psi}{2}\varphi\right) - 1\right)\right)^2. \quad (29)$$

Using the above coefficients and Equation (15) in Equation (22) yields

$$\wp_{5,3}(\chi,\tau) = \frac{26\sqrt{2}\hbar_2\sqrt{-\frac{(-11+\sqrt{105})\hbar_2}{\hbar_1^4}}\hbar_1^2 - \sqrt{2}\left(-\frac{(-11+\sqrt{105})\hbar_2}{\hbar_1^4}\right)^{3/2}\hbar_1^6}{240\hbar_2} -$$

$$\frac{i\mu\left(-\frac{(-11+\sqrt{105})\hbar_2}{\hbar_1^4}\right)^{1/4}\hbar_1^2}{2^{1/4}}\left(-\frac{\psi}{2\zeta}\left(\coth\left(\frac{\psi}{2}\varphi\right) - 1\right)\right) - \mu^2\hbar_1^2\left(-\frac{\psi}{2\zeta}\left(\coth\left(\frac{\psi}{2}\varphi\right) - 1\right)\right)^2.$$

**Case 6.** If $g_0 = 0$, $g_1 = \hbar_2^{1/4}\zeta\hbar_1$, $g_2 = -\zeta^2\hbar_1^2$, $\psi = \frac{\hbar_2^{1/4}}{\hbar_1}$, then the following solutions are obtained.
When $\zeta \neq 0$, using the above coefficients and Equation (12) in Equation (22) yields

$$\wp_{6,1}(\chi,\tau) = \hbar_2^{1/4}\zeta\hbar_1\left(\frac{\psi}{\zeta + \psi C \exp(\psi\varphi)}\right) - \zeta^2\hbar_1^2\left(\frac{\psi}{\zeta + \psi C \exp(\psi\varphi)}\right)^2.$$

Using the above coefficients and Equation (14) in Equation (22) yields

$$\wp_{6,2}(\chi,\tau) = \hbar_2^{1/4}\zeta\hbar_1\left(-\frac{\psi}{2\zeta}\left(\tanh\left(\frac{\psi}{2}\varphi\right) - 1\right)\right) - \zeta^2\hbar_1^2\left(-\frac{\psi}{2\zeta}\left(\tanh\left(\frac{\psi}{2}\varphi\right) - 1\right)\right)^2. \quad (30)$$

Using the above coefficients and Equation (15) in Equation (22) yields

$$\wp_{6,3}(\chi,\tau) = \hbar_2^{1/4}\zeta\hbar_1\left(-\frac{\psi}{2\zeta}\left(\coth\left(\frac{\psi}{2}\varphi\right) - 1\right)\right) - \zeta^2\hbar_1^2\left(-\frac{\psi}{2\zeta}\left(\coth\left(\frac{\psi}{2}\varphi\right) - 1\right)\right)^2.$$

**Case 7.** If $g_0 = 0$, $g_1 = \iota\hbar_2^{1/4}\zeta\hbar_1$, $g_2 = -\zeta^2\hbar_1^2$, $\psi = \frac{\iota\hbar_2^{1/4}}{\hbar_1}$, then the following solutions are obtained.

When $\zeta \neq 0$, using the above coefficients and Equation (12) in Equation (22) yields

$$\wp_{7,1}(\chi, \tau) = \imath \hbar_2^{1/4} \zeta \hbar_1 \left( \frac{\psi}{\zeta + \psi C \exp(\psi \varphi)} \right) - \zeta^2 \hbar_1^2 \left( \frac{\psi}{\zeta + \psi C \exp(\psi \varphi)} \right)^2.$$

Using the above coefficients and Equation (14) in Equation (22) yields

$$\wp_{7,2}(\chi, \tau) = \imath \hbar_2^{1/4} \zeta \hbar_1 \left( -\frac{\psi}{2\zeta} \left( \tanh \left( \frac{\psi}{2} \varphi \right) - 1 \right) \right) - \zeta^2 \hbar_1^2 \left( -\frac{\psi}{2\zeta} \left( \tanh \left( \frac{\psi}{2} \varphi \right) - 1 \right) \right)^2. \quad (31)$$

Using the above coefficients and Equation (15) in Equation (22) yields

$$\wp_{7,3}(\chi, \tau) = \imath \hbar_2^{1/4} \zeta \hbar_1 \left( -\frac{\psi}{2\zeta} \left( \coth \left( \frac{\psi}{2} \varphi \right) - 1 \right) \right) - \zeta^2 \hbar_1^2 \left( -\frac{\psi}{2\zeta} \left( \coth \left( \frac{\psi}{2} \varphi \right) - 1 \right) \right)^2.$$

*5.2. Sardar Sub-Equation Technique*

In this section, Sardar sub-equation technique [60] is applied to the CDGSK equation to construct the soliton wave solution. By the equilibrium rule, Equation (20) reduces into

$$N(\varphi) = r_0 + r_1 \Im(\varphi) + r_2 \Im(\varphi)^2, \quad (32)$$

where $r_0$, $r_1$, $r_2$ are constants. Substituting Equations (32) and (21) into Equation (6), we obtain

$$- \hbar_2 \hbar_1 r_0 + 60 \hbar_1 r_0^3 - \hbar_2 \hbar_1 \Im(\varphi) r_1 + u^2 \hbar_1^5 \Im(\varphi) r_1 + 12 f \hbar_1^5 \Im(\varphi) r_1 + 20 u \hbar_1^5 \Im(\varphi)^3 r_1 + 24 \hbar_1^5 \Im(\varphi)^5 r_1 +$$
$$30 u \hbar_1^3 \Im(\varphi) r_0 r_1 + 60 \hbar_1^3 \Im(\varphi)^3 r_0 r_1 + 180 \hbar_1 \Im(\varphi) r_0^2 r_1 + 30 u \hbar_1^3 \Im(\varphi)^2 r_1^2 + 60 \hbar_1^3 \Im(\varphi)^4 r_1^2 + 180 \hbar_1 \Im(\varphi)^2 r_0 r_1^2 +$$
$$60 \hbar_1 \Im(\varphi)^3 r_1^3 + 8 u f \hbar_1^5 r_2 - \hbar_2 \hbar_1 \Im(\varphi)^2 r_2 + 16 u^2 \hbar_1^5 \Im(\varphi)^2 r_2 + 72 f \hbar_1^5 \Im(\varphi)^2 r_2 + 120 u \hbar_1^5 \Im(\varphi)^4 r_2 + 120 \hbar_1^5 \Im(\varphi)^6 r_2 +$$
$$60 f \hbar_1^3 r_0 r_2 + 120 u \hbar_1^3 \Im(\varphi)^2 r_0 r_2 + 180 \hbar_1^3 \Im(\varphi)^4 r_0 r_2 + 180 \hbar_1 \Im(\varphi)^2 r_0^2 r_2 + 60 f \hbar_1^3 \Im(\varphi) r_1 r_2 + 150 u \hbar_1^3 \Im(\varphi)^3 r_1 r_2 +$$
$$240 \hbar_1^3 \Im(\varphi)^5 r_1 r_2 + 360 \hbar_1 \Im(\varphi)^3 r_0 r_1 r_2 + 180 \hbar_1 \Im(\varphi)^4 r_1^2 r_2 + 60 f \hbar_1^3 \Im(\varphi)^2 r_2^2 + 120 u \hbar_1^3 \Im(\varphi)^4 r_2^2 + 180 \hbar_1^3 \Im(\varphi)^6 r_2^2 +$$
$$180 \hbar_1 \Im(\varphi)^4 r_0 r_2^2 + 180 \hbar_1 \Im(\varphi)^5 r_1 r_2^2 + 60 \hbar_1 \Im(\varphi)^6 r_2^3 = 0. \quad (33)$$

After all the coefficients of $\Im(\varphi)^p$ are set to zero, the following set of algebraic Equations emerges:

$$\Im(\varphi)^0 : -\hbar_2 \hbar_1 r_0 + 60 \hbar_1 r_0^3 + 8 f u \hbar_1^5 r_2 + 60 f \hbar_1^3 r_0 r_2 = 0,$$
$$\Im(\varphi)^1 : -\hbar_2 \hbar_1 r_1 + u^2 \hbar_1^5 r_1 + 12 f \hbar_1^5 r_1 + 30 u \hbar_1^3 r_0 r_1 + 180 \hbar_1 r_0^2 r_1 + 60 f \hbar_1^3 r_1 r_2 = 0,$$
$$\Im(\varphi)^2 : 30 u \hbar_1^3 r_1^2 + 180 \hbar_1 r_0 r_1^2 - \hbar_2 \hbar_1 r_2 + 16 u^2 \hbar_1^5 r_2 + 72 f \hbar_1^5 r_2 + 120 u \hbar_1^3 r_0 r_2 + 180 \hbar_1 r_0^2 r_2 + 60 f \hbar_1^3 r_2^2 = 0,$$
$$\Im(\varphi)^3 : 20 u \hbar_1^5 r_1 + 60 \hbar_1^3 r_0 r_1 + 60 \hbar_1 r_1^3 + 150 u \hbar_1^3 r_1 r_2 + 360 \hbar_1 r_0 r_1 r_2 = 0,$$
$$\Im(\varphi)^4 : 60 \hbar_1^3 r_1^2 + 120 u \hbar_1^5 r_2 + 180 \hbar_1^3 r_0 r_2 + 180 \hbar_1 r_1^2 r_2 + 120 u \hbar_1^3 r_2^2 + 180 \hbar_1 r_0 r_2^2 = 0,$$
$$\Im(\varphi)^5 : 24 \hbar_1^5 r_1 + 240 \hbar_1^3 r_1 r_2 + 180 \hbar_1 r_1 r_2^2 = 0,$$
$$\Im(\varphi)^6 : 120 \hbar_1^5 r_2 + 180 \hbar_1^3 r_2^2 + 60 \hbar_1 r_2^3 = 0.$$
$$(34)$$

The following constants are found using Mathematica software, by solving the aforementioned Equations:

$$r_0 = -\frac{2u \hbar_1^2}{3}, \quad r_1 = 0, \quad r_2 = -2\hbar_1^2, \quad \hbar_2 = 16 \left( u^2 \hbar_1^4 - 3 f \hbar_1^4 \right). \quad (35)$$

The following answers are built using Equations (21), (32), and (35) in conjunction with Equation (4).

**Set 1:** if $u > 0$ and $f = 0$, then by using Equation (35), the analytical solution of Equation (32) is as follows:

$$N_1(\chi, \tau) = -\frac{2u\hbar_1^2}{3} - 2\hbar_1^2\left(\sqrt{-lmu}\,\text{sech}_{lm}\left(\sqrt{u}\varphi\right)\right)^2, \tag{36}$$

$$N_2(\chi, \tau) = -\frac{2u\hbar_1^2}{3} - 2\hbar_1^2\left(\sqrt{lmu}\,\text{csch}_{lm}\left(\sqrt{u}\varphi\right)\right)^2. \tag{37}$$

**Set 2:** if $u < 0$ and $f = 0$, then by using Equation (35), the analytical solution of Equation (32) is as follows:

$$N_3(\chi, \tau) = -\frac{2u\hbar_1^2}{3} - 2\hbar_1^2\left(\sqrt{-lmu}\,\sec_{lm}\left(\sqrt{-u}\varphi\right)\right)^2, \tag{38}$$

$$N_4(\chi, \tau) = -\frac{2u\hbar_1^2}{3} - 2\hbar_1^2\left(\sqrt{-lmu}\,\csc_{lm}\left(\sqrt{-u}\varphi\right)\right)^2. \tag{39}$$

**Set 3:** if $u < 0$ and $f = \frac{u^2}{4}$, then by using Equation (35), the analytical solution of Equation (32) is as follows:

$$N_5(\chi, \tau) = -\frac{2u\hbar_1^2}{3} - 2\hbar_1^2\left(\sqrt{\frac{-u}{2}}\,\tanh_{lm}\left(\sqrt{\frac{-u}{2}}\varphi\right)\right)^2, \tag{40}$$

$$N_6(\chi, \tau) = -\frac{2u\hbar_1^2}{3} - 2\hbar_1^2\left(\sqrt{\frac{-u}{2}}\,\coth_{lm}\left(\sqrt{\frac{-u}{2}}\varphi\right)\right)^2, \tag{41}$$

$$N_7(\chi, \tau) = -\frac{2u\hbar_1^2}{3} - 2\hbar_1^2\left(\sqrt{\frac{-u}{2}}\left(\tanh_{lm}(\sqrt{-2u}\varphi) + \iota\sqrt{lm}\,\text{sech}_{lm}\left(\sqrt{-2u}\varphi\right)\right)\right)^2, \tag{42}$$

$$N_8(\chi, \tau) = -\frac{2u\hbar_1^2}{3} - 2\hbar_1^2\left(\sqrt{\frac{-u}{2}}\left(\coth_{lm}(\sqrt{-2u}\varphi) + \iota\sqrt{lm}\,\text{csch}_{lm}\left(\sqrt{-2u}\varphi\right)\right)\right)^2, \tag{43}$$

$$N_9(\chi, \tau) = -\frac{2u\hbar_1^2}{3} - 2\hbar_1^2\left(\sqrt{\frac{-u}{8}}\left(\tanh_{lm}(\sqrt{\frac{-u}{8}}\varphi) + \coth_{lm}\left(\sqrt{\frac{-u}{8}}\varphi\right)\right)\right)^2. \tag{44}$$

**Set 4:** if $u > 0$ and $f = \frac{u^2}{4}$, then by using Equation (35), the analytical solution of Equation (32) is as follows:

$$N_{10}(\chi, \tau) = -\frac{2u\hbar_1^2}{3} - 2\hbar_1^2\left(\sqrt{\frac{u}{2}}\,\tan_{lm}\left(\sqrt{\frac{u}{2}}\varphi\right)\right)^2, \tag{45}$$

$$N_{11}(\chi, \tau) = -\frac{2u\hbar_1^2}{3} - 2\hbar_1^2\left(\sqrt{\frac{u}{2}}\,\cot_{lm}\left(\sqrt{\frac{u}{2}}\varphi\right)\right)^2, \tag{46}$$

$$N_{12}(\chi, \tau) = -\frac{2u\hbar_1^2}{3} - 2\hbar_1^2\left(\sqrt{\frac{u}{2}}\left(\tan_{lm}\left(\sqrt{2u}\varphi\right) + \sqrt{lm}\,\sec_{lm}\left(\sqrt{2u}\varphi\right)\right)\right)^2, \tag{47}$$

$$N_{13}(\chi, \tau) = -\frac{2u\hbar_1^2}{3} - 2\hbar_1^2\left(\sqrt{\frac{u}{2}}\left(\cot_{lm}\left(\sqrt{2u}\varphi\right) + \sqrt{lm}\,\csc_{lm}\left(\sqrt{2u}\varphi\right)\right)\right)^2, \tag{48}$$

$$N_{14}(\chi, \tau) = -\frac{2u\hbar_1^2}{3} - 2\hbar_1^2\left(\sqrt{\frac{u}{8}}\left(\tan_{lm}\left(\sqrt{\frac{u}{8}}\varphi\right) + \cot_{lm}\left(\sqrt{\frac{u}{8}}\varphi\right)\right)\right)^2. \tag{49}$$

## 6. Results and Discussion

In this work, the CDGSK model has been analytically solved using fractional operators by employing Jumarie's modified RL derivative. To find these solutions, the BSOM approaches and the successful SSET strategy were employed. Multiple outcomes have been generated by the approaches, and 2D graphs have been utilized for evaluating the answers acquired for derivative operators. The methods outlined above can be used to create solitary waves in a range of forms, such as multiwave, kink, smooth-bell-shaped, and anti-bell-shaped soliton, W-shaped, M-shaped, periodic, bright singular, and dark singular solitons, and combined dark and bright solitons. When the value of the fractional parameter is changed, it can be seen that the solitary wave is somewhat altered without changing the shape of the curve. With varying parameter values, Figures 1–6 depict the different soliton solutions of $\wp_{1,2}(\chi, \tau)$, $\wp_{2,2}(\chi, \tau)$, $\wp_{3,2}(\chi, \tau)$, $\wp_{5,2}(\chi, \tau)$, $\wp_{6,2}(\chi, \tau)$, and $\wp_{7,2}(\chi, \tau)$ as solved by the BSOM technique. When we consider the values of $\alpha = 0.9$, $\hbar_1 = -2$, $\psi = -0.35$, $\zeta = -0.95$, $\tau = 10$ within the range $-10 \leq \chi \leq 10, 2 \leq \tau \leq 3$, as seen in Figure 1, we find the bright soliton solutions for the 2D and 3D graphs of $\wp_{1,2}(\chi, \tau)$. When we consider the values of $\alpha = 1$, $\hbar_2 = 0.75$, $\psi = 0.25$, $\zeta = 0.5$, $\tau = 10$ within the range $-10 \leq \chi \leq 10, 1 \leq \tau \leq 2$, as seen in Figure 2, we find the anti-kink soliton solutions for the 2D and 3D graphs of $\wp_{2,2}(\chi, \tau)$. When we consider the values of $\alpha = 1$, $\hbar_2 = -0.08$, $\psi = -0.5$, $\zeta = -0.75$, $\tau = 10$ within the range $-15 \leq \chi \leq 15, 4 \leq \tau \leq 5$, as seen in Figure 3, we find the M-shaped soliton solutions for the 2D and 3D graphs of $\wp_{3,2}(\chi, \tau)$. When we consider the values of $\alpha = 1$, $\hbar_1 = -2$, $\hbar_2 = -0.25$, $\zeta = -5$, $\tau = 20$ within the range $-10 \leq \chi \leq 10, 1 \leq \tau \leq 2$, as seen in Figure 4, we find the M-shaped soliton solutions for the 2D and 3D graphs of $\wp_{5,2}(\chi, \tau)$. When we consider the values of $\alpha = 0.5$, $\hbar_1 = 10$, $\hbar_2 = -10$, $\zeta = 1$, $\tau = 8$ within the range $-10 \leq \chi \leq 10, 1 \leq \tau \leq 2$, as seen in Figure 5, we find the soliton solutions for the 2D and 3D graphs of $\wp_{6,2}(\chi, \tau)$. When we consider the values of $\alpha = 1$, $\hbar_1 = -4$, $\hbar_2 = -5$, $\zeta = -2$, $\tau = 5$ within the range $-4 \leq \chi \leq 7, 1 \leq \tau \leq 2$, as seen in Figure 6, we find the M-shaped soliton solutions for the 2D and 3D graphs of $\wp_{7,2}(\chi, \tau)$. With varying parameter values, Figure 7–18 depict the different soliton solutions of $N_1(\chi, \tau)$, $N_2(\chi, \tau)$, $N_3(\chi, \tau)$, $N_4(\chi, \tau)$, $N_5(\chi, \tau)$, $N_6(\chi, \tau)$, $N_7(\chi, \tau)$, $N_8(\chi, \tau)$, $N_9(\chi, \tau)$, $N_{11}(\chi, \tau)$, $N_{13}(\chi, \tau)$, and $N_{14}(\chi, \tau)$ as solved by the SSET technique. Figure 7 illustrates the W-shaped soliton for parameters $u = 0.2$, $\alpha = 1$, $\hbar_1 = 1$, $f = 0$, $l = 0.25$, $m = 0.75$, $\tau = 5$ in the range of $-5 \leq \chi \leq 10, 1 \leq \tau \leq 2$, and $\tau = 1, 2, 3$ for 2D plots. Figure 8 illustrates the bright singular soliton for parameters $u = 0.2$, $\alpha = 1$, $\hbar_1 = 1$, $f = 0$, $l = 0.25$, $m = 0.75$, $\tau = 5$ in the range of $-5 \leq \chi \leq 10, 1 \leq \tau \leq 5$, and $\tau = 1, 2, 3$ for 2D plots. Figure 9 illustrates the periodic soliton for parameters $u = 0.2$, $\alpha = 1$, $\hbar_1 = 1$, $f = 0$, $l = 0.25$, $m = 0.75$, $\tau = 5$ in the range of $-10 \leq \chi \leq 10, 0 \leq \tau \leq 1$, and $\tau = 1, 2, 3$ for 2D plots. Figure 10 illustrates the anti-bell-shaped soliton for parameters $u = -0.3$, $\alpha = 1$, $\hbar_1 = -0.3$, $f = 0$, $l = -0.35$, $m = -0.5$, $\tau = 20$ in the range of $-5 \leq \chi \leq 5, 2 \leq \tau \leq 3$, and $\tau = 0, 10, 20$ for 2D plots. Figure 11 illustrates the W-shaped soliton for parameters $u = -0.6$, $\alpha = 1$, $\hbar_1 = 1$, $l = 0.25$, $m = 0.75$, $\tau = 5$ in the range of $-1 \leq \chi \leq 10, 2 \leq \tau \leq 3$, and $\tau = 1, 2, 3$ for 2D plots. Figure 12 illustrates the W-shaped soliton for parameters $u = -1$, $\alpha = 0.9$, $\hbar_1 = -1$, $l = 0.25$, $m = -10$, $\tau = 0.3$ in the range of $-13 \leq \chi \leq 5$, $0 \leq \tau \leq 1$, and $\tau = 0.1, 0.2, 0.3$ for 2D plots. Figure 13 illustrates the combined dark and bright soliton for parameters $u = -0.1$, $\alpha = 0.5$, $\hbar_1 = -3$, $l = 0.25$, $m = 0.75$, $\tau = 3$ in the range of $-7 \leq \chi \leq 3, 1 \leq \tau \leq 5$, and $\tau = 1, 2, 3$ for 2D plots. Figure 14 illustrates the combined dark and bright soliton for parameters $u = -0.3$, $\alpha = 1$, $\hbar_1 = -2$, $l = -5$, $m = 0.1$, $\tau = 0.3$ in the range of $-6 \leq \chi \leq 6, 0 \leq \tau \leq 1$, and $\tau = 0.1, 0.2, 0.3$ for 2D plots. Figure 15 illustrates the singular dark soliton for parameters $u = -0.3$, $\alpha = 0.9$, $\hbar_1 = -1$, $l = 10$, $m = -0.01$, $\tau = 4$ in the range of $15 \leq \chi \leq 20, 0 \leq \tau \leq 4$, and $\tau = 1, 2, 3$ for 2D plots. Figure 16 illustrates the periodic soliton for parameters $u = 1.1$, $\alpha = 1$, $\hbar_1 = -0.95$, $l = -0.25$, $m = 1$, $\tau = 3$ in the range of $-10 \leq \chi \leq 10, 0 \leq \tau \leq 5$, and $\tau = 1, 2, 3$ for 2D plots. Figure 17 illustrates the periodic soliton for parameters $u = 0.3$, $\alpha = 1$, $\hbar_1 = 0.9$, $l = 0.25$, $m = -0.75$, $\tau = 8$ in the range of $-10 \leq \chi \leq 12, 1 \leq \tau \leq 2$, and $\tau = 1, 3, 5$ for

2D plots. Figure 18 illustrates the gap soliton for parameters $u = 1$, $\alpha = 1$, $\hbar_1 = 0.85$, $l = 0.25$, $m = -0.95$, $\tau = 3$ in the range of $-10 \leq \chi \leq 10, 0 \leq \tau \leq 1$, and $\tau = 1, 3, 5$ for 2D plots. It should be noted that the value of $\alpha$ for variation in 2D plots is $\alpha = 0.75, 0.85, 0.95$ for all graphs.
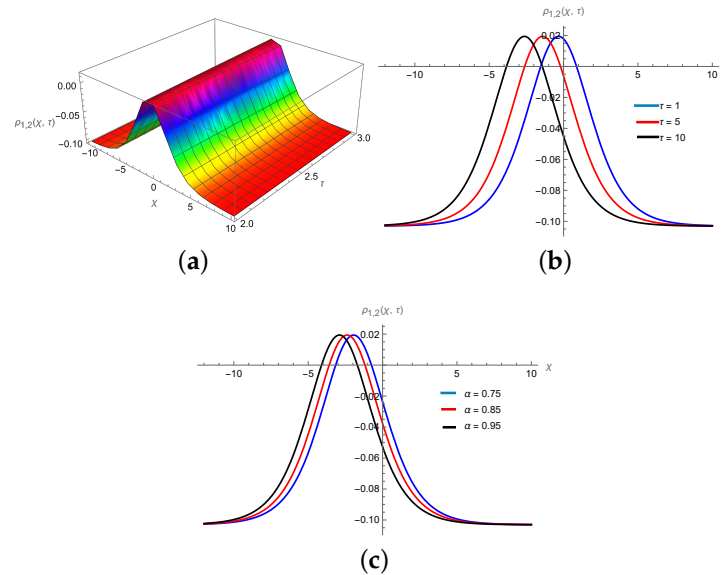


(a)



(b)



(c)

**Figure 1.** The analytical outcome of $\wp_{1,2}(\chi, \tau)$ by employing BSOM is bright soliton, when $\alpha = 0.9$, $\hbar_1 = -2$, $\psi = -0.35$, $\zeta = -0.95$: corresponding 2D plot of variation in $\alpha$ is at $t = 10$. (**a**) 3D Plot, (**b**) variation in $\tau$, (**c**) variation in $\alpha$.



(a)



(b)



(c)
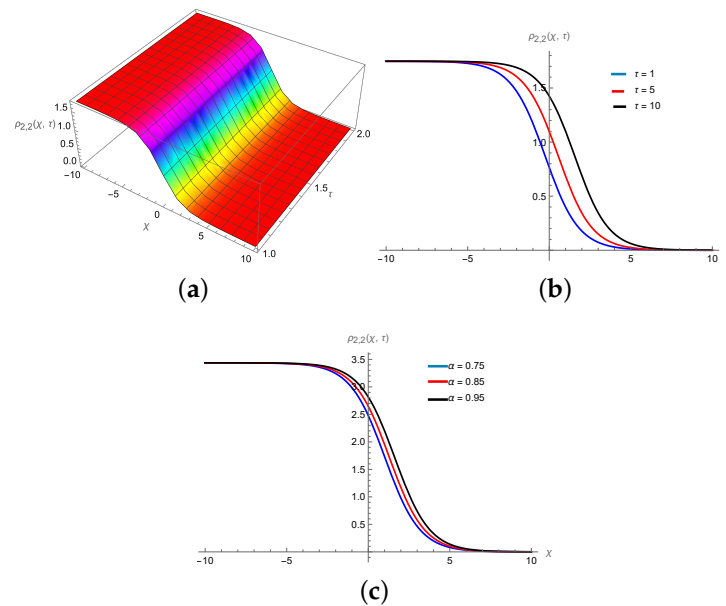
**Figure 2.** The analytical outcome of $\wp_{2,2}(\chi, \tau)$ by employing BSOM is anti-kink soliton, when $\alpha = 1$, $\hbar_2 = 0.75$, $\psi = 0.25$, $\zeta = 0.5$: corresponding 2D plot of variation in $\alpha$ is at $t = 10$. (**a**) 3D Plot, (**b**) variation in $\tau$, (**c**) variation in $\alpha$.
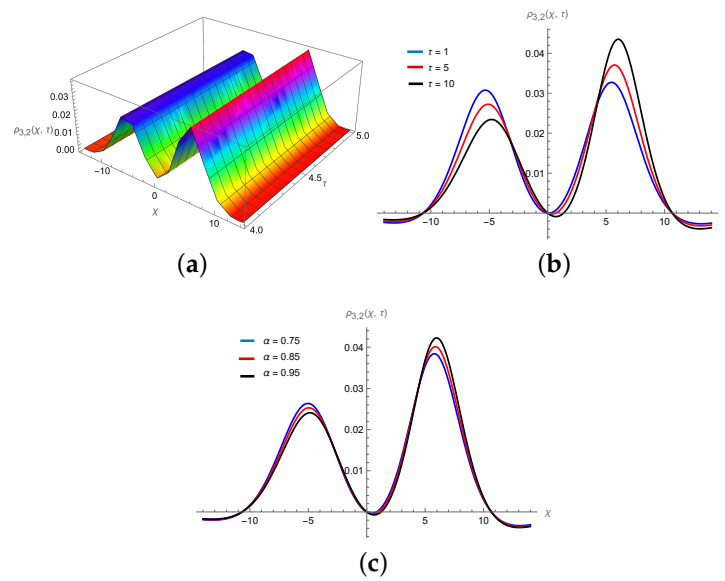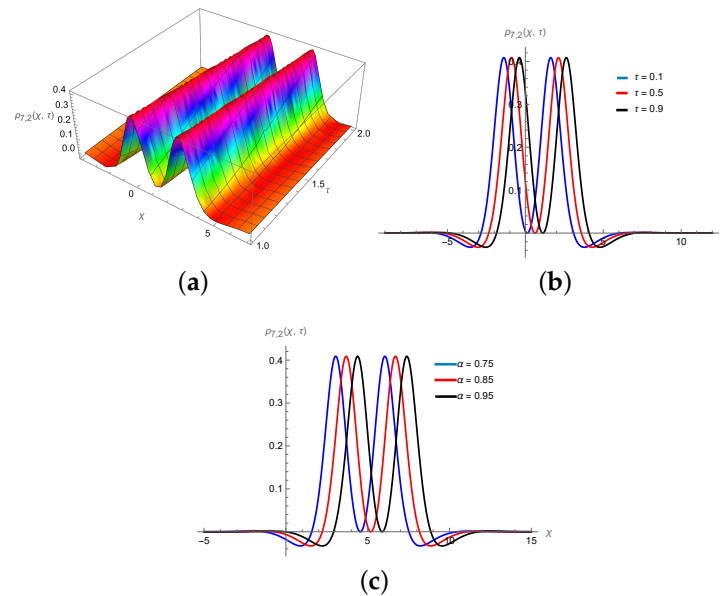
**Figure 3.** The analytical outcome of $\wp_{3,2}(\chi, \tau)$ by employing BSOM is M-shaped soliton, when $\alpha = 1$, $\hbar_2 = -0.08$, $\psi = -0.5$, $\zeta = -0.75$: corresponding 2D plot of variation in $\alpha$ is at $t = 10$. (**a**) 3D Plot, (**b**) variation in $\tau$, (**c**) variation in $\alpha$.
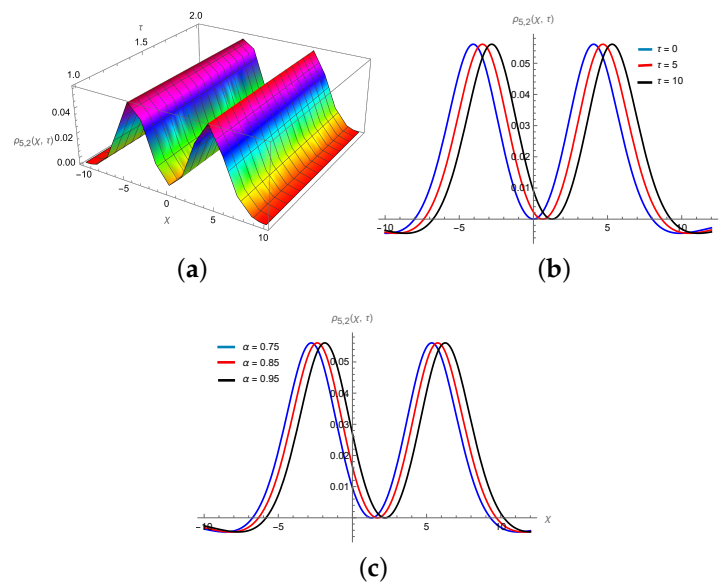


**Figure 4.** The analytical outcome of $\wp_{5,2}(\chi, \tau)$ by employing BSOM is M-shaped soliton, when $\alpha = 1$, $\hbar_1 = -2$, $\hbar_2 = -0.25$, $\zeta = -5$: corresponding 2D plot of variation in $\alpha$ is at $t = 20$. (**a**) 3D Plot, (**b**) variation in $\tau$, (**c**) variation in $\alpha$.

(a)

(b)

(c)
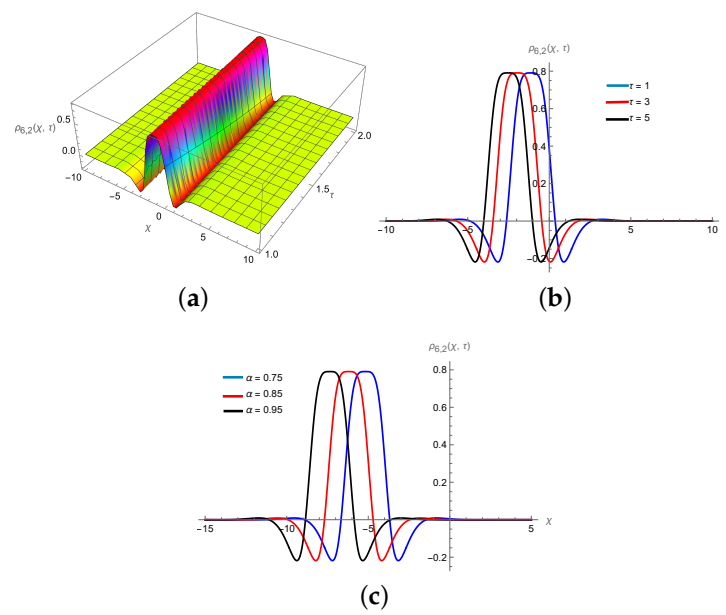
**Figure 5.** The analytical outcome of $\wp_{6,2}(\chi, \tau)$ by employing BSOM, when $\alpha = 0.5$, $\hbar_1 = 10$, $\hbar_2 = -10$, $\zeta = 1$: corresponding 2D plot of variation in $\alpha$ is at $t = 8$. (**a**) 3D Plot, (**b**) variation in $\tau$, (**c**) variation in $\alpha$.



(a)

(b)

(c)

**Figure 6.** The analytical outcome of $\wp_{5,2}(\chi, \tau)$ by employing BSOM is M-shaped soliton, when $\alpha = 1$, $\hbar_1 = -4$, $\hbar_2 = -5$, $\zeta = -2$: corresponding 2D plot of variation in $\alpha$ is at $t = 5$. (**a**) 3D Plot, (**b**) variation in $\tau$, (**c**) variation in $\alpha$.
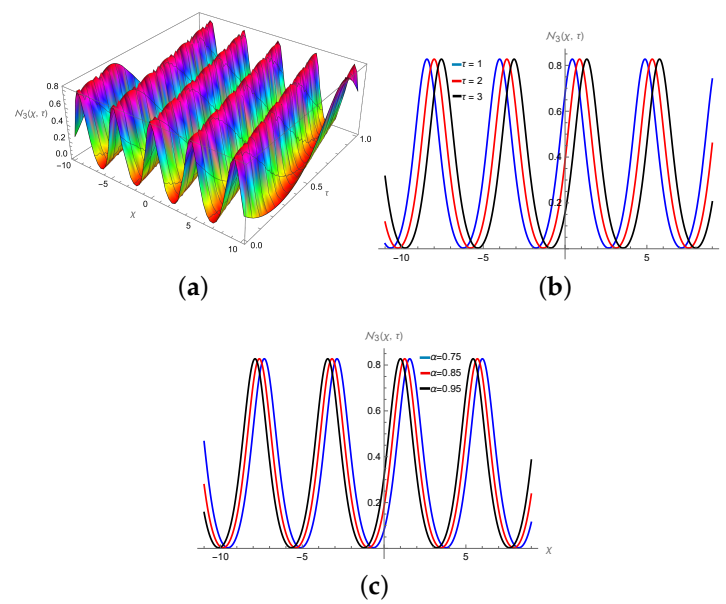
**(a)**



**(b)**



**(c)**
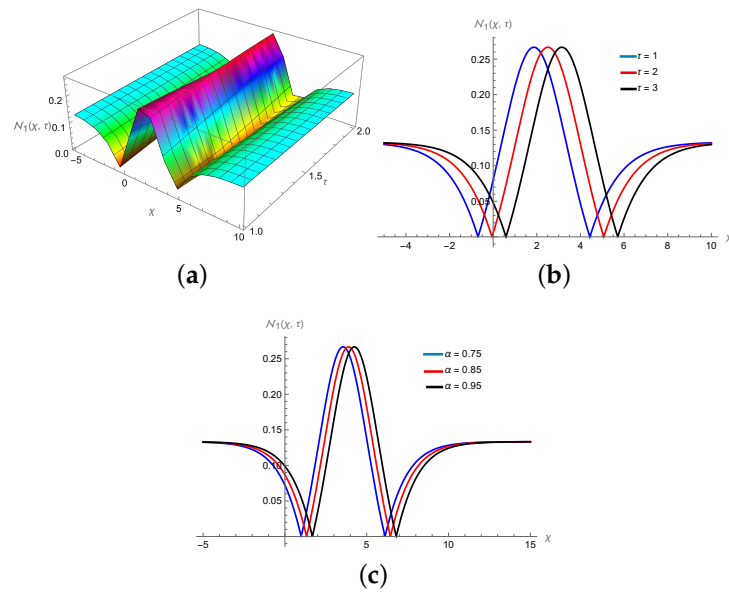
**Figure 7.** The W-shaped profile of the CDGSK equation corresponds to the solution $N_1(\chi, \tau)$ for the values of $u = 0.2$, $\alpha = 1$, $\hbar_1 = 1$, $f = 0$, $l = 0.25$, $m = 0.75$: corresponding 2D plot of variation in $\alpha$ is at $t = 5$. (**a**) 3D Plot, (**b**) variation in $\tau$, (**c**) variation in $\alpha$.
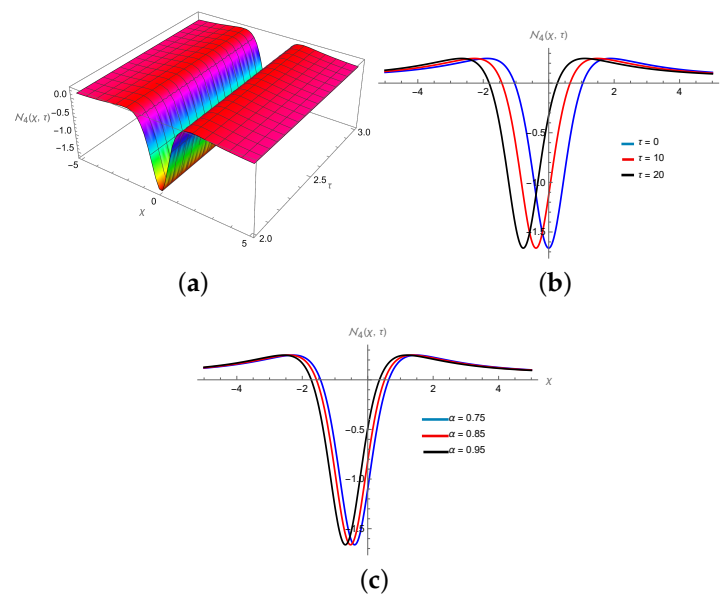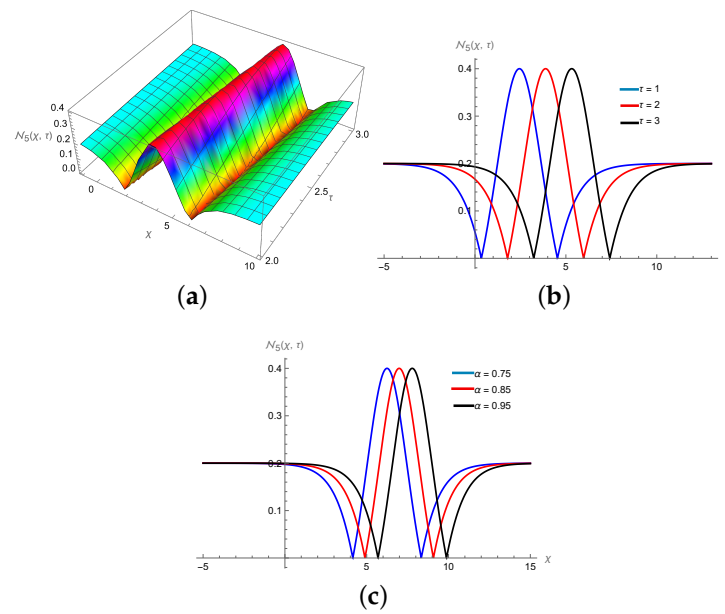


**(a)**



**(b)**



**(c)**
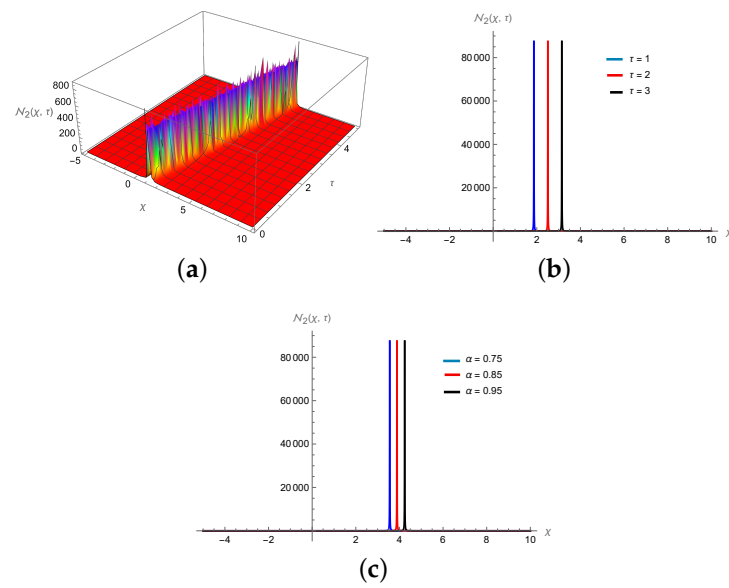
**Figure 8.** The bright singular profile of the CDGSK equation corresponds to the solution $N_2(\chi, \tau)$ for the values of $u = 0.2$, $\alpha = 1$, $\hbar_1 = 1$, $f = 0$, $l = 0.25$, $m = 0.75$: corresponding 2D plot of variation in $\alpha$ is at $t = 5$. (**a**) 3D Plot, (**b**) variation in $\tau$, (**c**) variation in $\alpha$.

(a)

(b)

(c)

**Figure 9.** The multiwave profile of the CDGSK equation corresponds to the solution $N_3(\chi, \tau)$ for the values of $u = -0.5$, $\alpha = 1$, $\hbar_1 = -1$, $f = 0$, $l = 0.1$, $m = -1$: corresponding 2D plot of variation in $\alpha$ is at $t = 2$. (**a**) 3D Plot, (**b**) variation in $\tau$, (**c**) variation in $\alpha$.
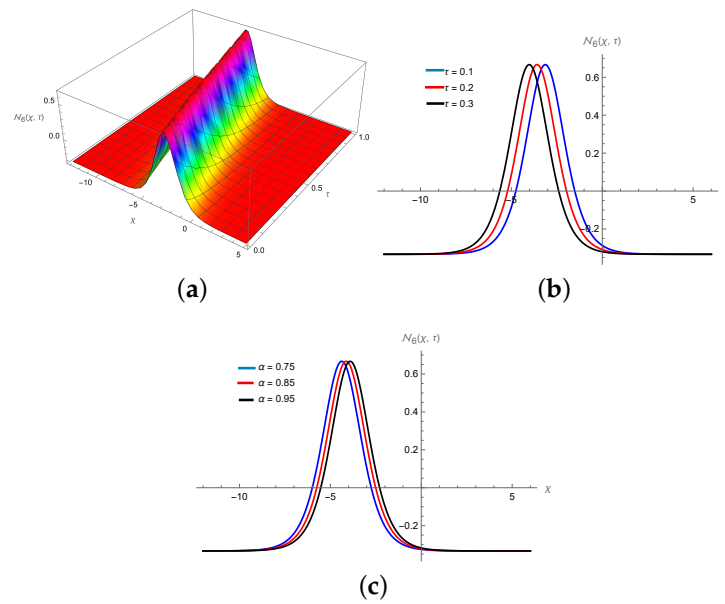


(a)

(b)

(c)

**Figure 10.** The anti-bell-shaped profile of the CDGSK equation corresponds to the solution $N_4(\chi, \tau)$ for the values of $u = -0.3$, $\alpha = 1$, $\hbar_1 = -0.3$, $f = 0$, $l = -0.35$, $m = -0.5$: corresponding 2D plot of variation in $\alpha$ is at $t = 20$. (**a**) 3D Plot, (**b**) variation in $\tau$, (**c**) variation in $\alpha$.

**(a)**



**(b)**



**(c)**

**Figure 11.** The W-shaped profile of the CDGSK equation corresponds to the solution $N_5(\chi, \tau)$ for the values of $u = -0.6$, $\alpha = 1$, $\hbar_1 = 1$, $l = 0.25$, $m = 0.75$: corresponding 2D plot of variation in $\alpha$ is at $t = 5$. (**a**) 3D Plot, (**b**) variation in $\tau$, (**c**) variation in $\alpha$.



**(a)**



**(b)**



**(c)**

**Figure 12.** The smooth-bell-shaped profile of the CDGSK equation corresponds to the solution $N_6(\chi, \tau)$ for the values of $u = -1$, $\alpha = 0.9$, $\hbar_1 = -1$, $l = 0.25$, $m = -10$: corresponding 2D plot of variation in $\alpha$ is at $t = 0.3$. (**a**) 3D Plot, (**b**) variation in $\tau$, (**c**) variation in $\alpha$.
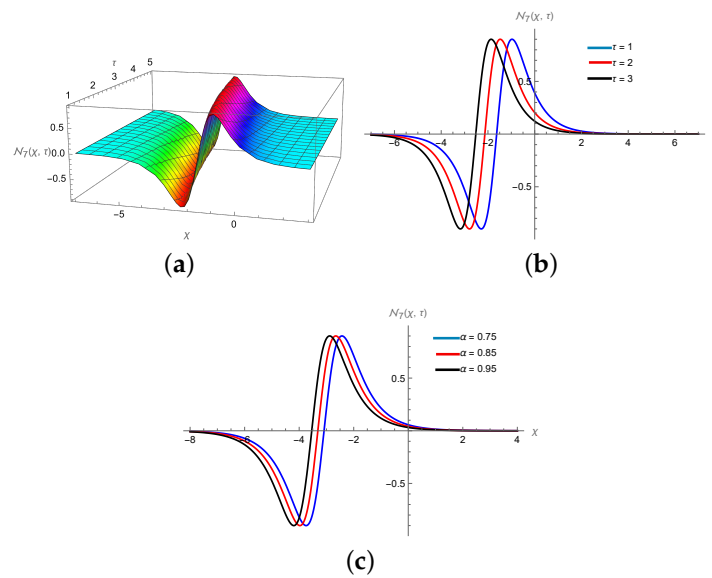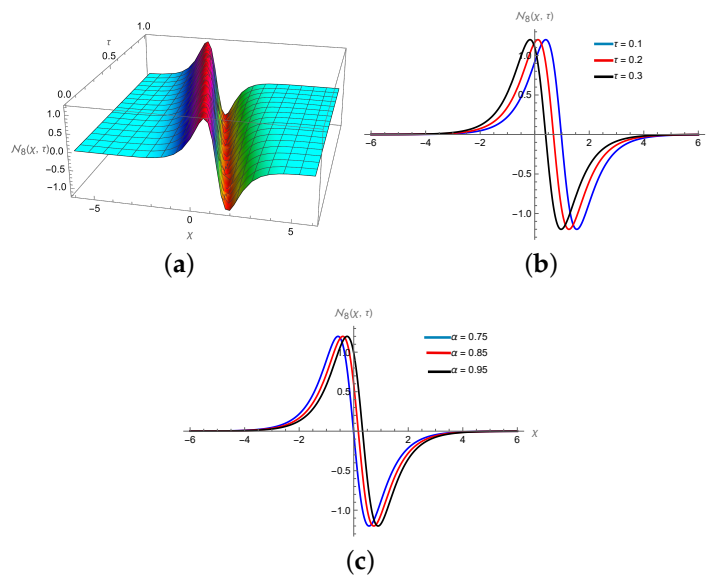
**Figure 13.** The combined dark and bright profile of the CDGSK equation corresponds to the solution $N_7(\chi, \tau)$ for the values of $u = -0.1$, $\alpha = 0.5$, $\hbar_1 = -3$, $l = 0.25$, $m = 0.75$: corresponding 2D plot of variation in $\alpha$ is at $t = 3$. (**a**) 3D Plot, (**b**) variation in $\tau$, (**c**) variation in $\alpha$.



**Figure 14.** The combined bright and dark profile of the CDGSK equation corresponds to the solution $N_8(\chi, \tau)$ for the values of $u = -0.3$, $\alpha = 1$, $\hbar_1 = -2$, $l = -5$, $m = 0.1$: corresponding 2D plot of variation in $\alpha$ is at $t = 0.3$. (**a**) 3D Plot, (**b**) variation in $\tau$, (**c**) variation in $\alpha$.
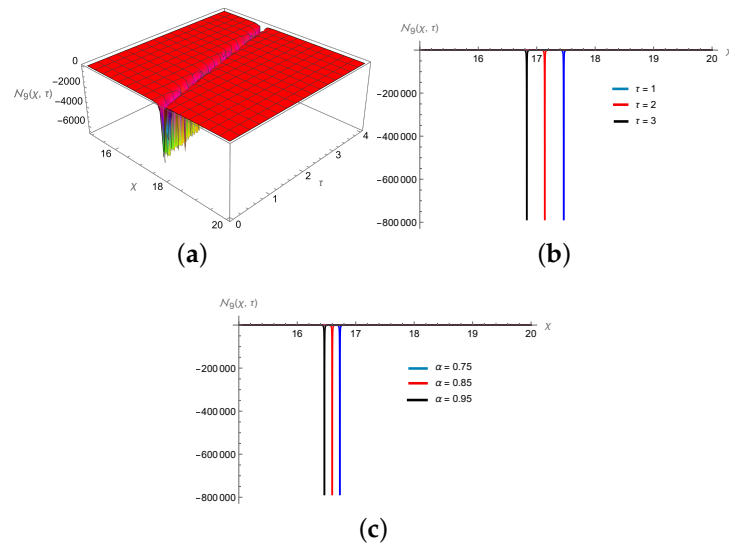
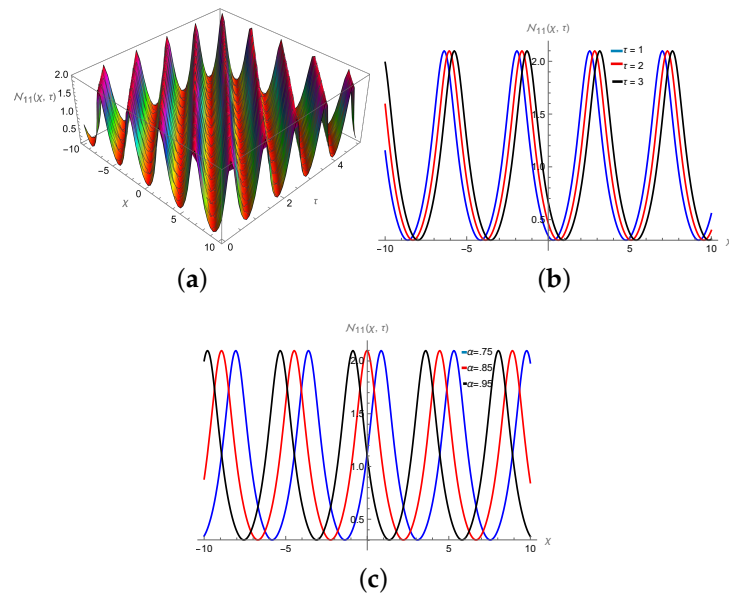**Figure 15.** The singular dark profile of the CDGSK equation corresponds to the solution $N_9(\chi, \tau)$ for the values of $u = -0.3$, $\alpha = 0.9$, $\hbar_1 = -1$, $l = 10$, $m = -0.01$: corresponding 2D plot of variation in $\alpha$ is at $t = 4$. (**a**) 3D Plot, (**b**) variation in $\tau$, (**c**) variation in $\alpha$.
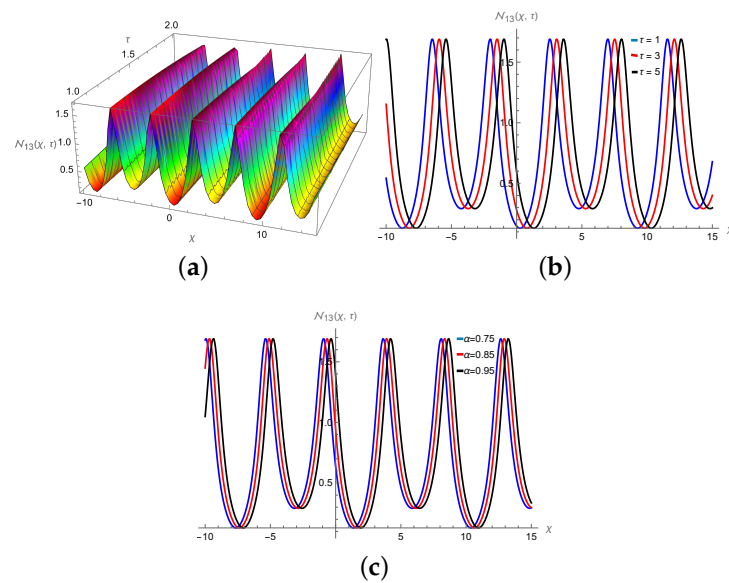


**Figure 16.** The periodic profile of the CDGSK equation corresponds to the solution $N_{11}(\chi, \tau)$ for the values of $u = 1.1$, $\alpha = 1$, $\hbar_1 = -0.95$, $l = -0.25$, $m = 1$: corresponding 2D plot of variation in $\alpha$ is at $t = 3$. (**a**) 3D Plot, (**b**) variation in $\tau$, (**c**) variation in $\alpha$.

**Figure 17.** The periodic profile of the CDGSK equation corresponds to the solution $N_{13}(\chi, \tau)$ for the values of $u = 0.3$, $\alpha = 1$, $\hbar_1 = 0.9$, $l = 0.25$, $m = -0.75$: corresponding 2D plot of variation in $\alpha$ is at $t = 8$. (**a**) 3D Plot, (**b**) variation in $\tau$, (**c**) variation in $\alpha$.
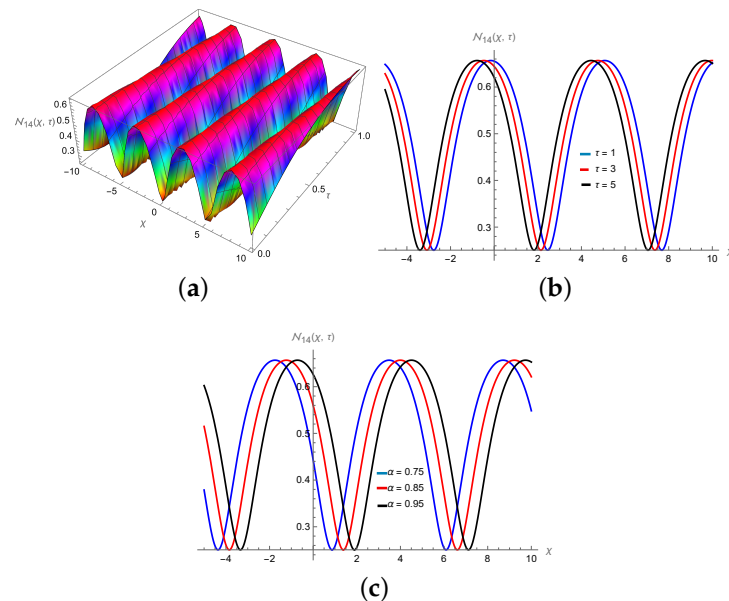


**Figure 18.** The gap soliton of the CDGSK equation corresponds to the solution $N_{14}(\chi, \tau)$ for the values of $u = 1$, $\alpha = 1$, $\hbar_1 = 0.85$, $l = 0.25$, $m = -0.95$: corresponding 2D plot of variation in $\alpha$ is at $t = 3$. (**a**) 3D Plot, (**b**) variation in $\tau$, (**c**) variation in $\alpha$.

## 7. Comparison of the Results

This section of the paper attempts to investigate a comparison between the solutions available in previous literature and the findings of the fractional nonlinear CDGSK problem obtained by the introduced approaches. By using the new auxiliary equation method, Adil et al. [49] obtained dark, bright, singular, and periodic soliton using the values of fractional parameter $\gamma$ between 0.3 to 0.9, with Beta and Atangana–Baleanu fractional derivatives. Also, Dumitru et al. [53] employed Lie symmetry analysis and sub-equation method to find the exact solutions of the time-fractional CDGSK equation with the Riemann–

Liouville derivative. In this study, the analytical solution pertaining to the fractional CDGSK equation, using Jumarie's modified RLD in conjunction with the BSOM and SSET technique, we get gap, multiwave and periodic waves, bell, anti-bell shaped, W-shaped, M-shaped, singular bright and singular dark waves, combined bright and dark solitons, and anti-kink waves by taking different values of fractional parameter $\alpha$ such as $0.75, 0.85, 0.95$.

## 8. Painlevé Analysis

For evaluating the integrability of nonlinear PDEs, Painlevé analysis [56,61] is a popular analytical technique. The methods that are most frequently used to prove the Painlevé property are Weiss–Tabor–Carnevale (WTC) and Kruskal's simplification approach. There are three primary steps involved in applying the WTC–Kruskal algorithm:

1. Investigating the leading-order analysis;
2. Finding resonances;
3. Figuring out the requirements for compatibility.

If there are single-valued solutions to the time fractional CDGSK equation about movable singularity manifolds that are arbitrary and non-characteristic, then the equation is said to have the Painlevé property. For this, consider the generalized fifth-order CDGSK equation:

$$\wp_t + \wp_{\chi\chi\chi\chi\chi} + (a_1\wp^3 + a_2\wp\wp_{\chi\chi} + a_3\wp_\chi^2)_\chi = 0, \tag{50}$$

where $a_1, a_2, a_3$ are arbitrary constants. Equation (50) may be reduced into Equation (1) for $a_1 = 60, a_2 = 30$ and $a_3 = 0$, respectively. In this study, we aim to find a Laurent series expansion about a singular manifold $\eta(\chi, \tau)$ as a solution of Equation (50).

$$\wp(\chi, \tau) = \sum_{r=0}^{\infty} \wp_r(\chi, \tau)\eta^{r-y}, \quad where \; r = 0, 1, 2, \ldots \tag{51}$$

where $y$ is a non-negative integer, and $\wp_r(\chi, \tau)$ are the functions of $\chi$ and $\tau$. Equating the terms that are most prevalent after plugging Equation (51) into Equation (50) yields $r = 2$, and the related resonances $r$ of leading order behaviors are

$$\wp_0(\chi, \tau) = -\frac{3a_2\eta_\chi^2 + 2a_3\eta_\chi^2 \pm \sqrt{(-120a_1 + 9a_2^2 + 12a_2a_3 + 4a_3^2)\eta_\chi^4}}{a}; \quad r = -1, 6, \Delta, \tag{52}$$

where the set of resonances denoted by $\Delta$ depends on the constants $a_1, a_2, a_3$. It is studied as follows, for CDGSK equation with $a_1 = 60, a_2 = 30, a_3 = 0$

$$\wp_0 = -2\eta_\chi^2; \qquad r = -1, 5, 6, 12,$$
$$\wp_0 = -\eta_\chi^2; \qquad r = -1, 2, 3, 6, 10.$$

The resonance $-1$ in the aforementioned expressions is in accordance with the irrational choice of the singular manifold $\eta(\chi, \tau) = 0$, and we found explicit formulations for $\wp_j; j = 1, 2, \ldots$, where some of the $\wp_j$ are arbitrary functions. Equation (50) satisfies the Painlevé test for complete integrability with the constraint on the parameters $a_1, a_2$, and $a_3$, and hence depends on the parameters. Additionally, compatibility conditions are satisfied similarly for the resonances $r$. The Painlevé test is said to be satisfied if the constants of integration $\wp_r$ at the resonances $r$ become arbitrary constants.

## 9. Conclusions

This study addresses the analytical solution pertaining to the fractional CDGSK equation. Using Jumarie's modified RLD in conjunction with the BSOM and SSET techniques, analytical solutions for the suggested equation have been produced. It is challenging to provide an integrated analytical approach for every kind of NLPDE. These recommended procedures are standard and computational approaches that enable us to carry out laborious

and complex algebraic computations. Both approaches work effectively and are frequently employed to deal with differential equations. The results show that, in comparison to the other approach, the SSET is more accurate and uses less computational power. It is capable of generating more solutions. Rational, hyperbolic, and trigonometric functions are the forms that the acquired results embrace. As a result, precise types of solitary waves such as gap, multiwave and periodic waves, bell, anti-bell shaped, W-shaped, M-shaped, singular bright and singular dark waves, combined bright and dark solitons, and anti-kink waves have been established. With the aid of Mathematica tools, Figures 1–18 have been generated to illustrate how the parametric variables, in particular $\alpha$ for different values, influence the shape of the soliton.

## References

1. Machado, J.T.; Kiryakova, V.; Mainardi, F. Recent history of fractional calculus. *Commun. Nonlinear Sci. Numer. Simul.* **2011**, *16*, 1140–1153. [CrossRef]
2. Hilfer, R. (Ed.) *Applications of Fractional Calculus in Physics*; World Scientific: Singapore, 2000; pp. 3–6.
3. Butera, S.; Di Paola, M. A physically based connection between fractional calculus and fractal geometry. *Ann. Phys.* **2014**, *350*, 146–158. [CrossRef]
4. Diethelm, K.; Ford, N.J. Analysis of fractional differential equations. *J. Math. Anal. Appl.* **2002**, *265*, 229–248. [CrossRef]
5. Cattani, C.; Srivastava, H.M.; Yang, X.J. (Eds.) *Fractional Dynamics*; Walter de Gruyter GmbH & Co KG: Berlin, Germany, 2015.
6. Dalir, M.; Bashour, M. Applications of fractional calculus. *Appl. Math. Sci.* **2010**, *4*, 1021–1032.
7. Wang, H. Research on application of fractional calculus in signal real-time analysis and processing in stock financial market. *Chaos Solitons Fractals* **2019**, *128*, 92–97. [CrossRef]
8. Ghasemi, S.; Tabesh, A.; Askari-Marnani, J. Application of fractional calculus theory to robust controller design for wind turbine generators. *IEEE Trans. Energy Convers.* **2014**, *29*, 780–787. [CrossRef]
9. Adomian, G. A new approach to nonlinear partial differential equations. *J. Math. Anal. Appl.* **1984**, *102*, 420–434. [CrossRef]
10. Raissi, M.; Karniadakis, G.E. Hidden physics models: Machine learning of nonlinear partial differential equations. *J. Comput. Phys.* **2018**, *357*, 125–141. [CrossRef]
11. Antontsev, S.N.; Díaz, J.I.; Shmarev, S.; Kassab, A.J. Energy Methods for Free Boundary Problems: Applications to Nonlinear PDEs and Fluid Mechanics. Progress in Nonlinear Differential Equations and Their Applications, Vol 48. *Appl. Mech. Rev.* **2002**, *55*, B74–B75. [CrossRef]
12. Ghergu, M.; Radulescu, V. *Nonlinear PDEs: Mathematical Models in Biology, Chemistry and Population Genetics*; Springer Science & Business Media: Berlin/Heidelberg, Germany, 2011.
13. Raissi, M. Deep hidden physics models: Deep learning of nonlinear partial differential equations. *J. Mach. Learn. Res.* **2018**, *19*, 1–24.
14. Yuan, T.; Zhu, J.; Wang, W.; Lu, J.; Wang, X.; Li, X.; Ren, K. A space-time partial differential equation based physics-guided neural network for sea surface temperature prediction. *Remote Sens.* **2023**, *15*, 3498. [CrossRef]
15. Abou-Dina, M.S.; Helal, M.A. Reduction for the nonlinear problem of fluid waves to a system of integro-differential equations with an oceanographical application. *J. Comput. Appl. Math.* **1998**, *95*, 65–81. [CrossRef]
16. Selvam, A.M.; Selvam, A.M. Nonlinear dynamics and chaos: Applications in meteorology and atmospheric physics. In *Self-Organized Criticality and Predictability in Atmospheric Flows: The Quantum World of Clouds and Rain*; Springer: Berlin/Heidelberg, Germany, 2017; pp. 1–40.
17. Roubíček, T. *Nonlinear Partial Differential Equations with Applications*; Springer Science & Business Media: Berlin/Heidelberg, Germany, 2013; Volume 153.

18. Remoissenet, M. *Waves Called Solitons: Concepts and Experiments*; Springer Science & Business Media: Berlin/Heidelberg, Germany, 2013; pp. 1–11.

19. Wadati, M. Introduction to solitons. *Pramana* **2001**, *57*, 841–847. [CrossRef]

20. Wazwaz, A.M. Multiple-soliton solutions for the KP equation by Hirota's bilinear method and by the tanh–coth method. *Appl. Math. Comput.* **2007**, *190*, 633–640. [CrossRef]

21. Fokas, A.S. A unified transform method for solving linear and certain nonlinear PDEs. *Proc. R. Soc. Lond. Ser. Math. Phys. Eng. Sci.* **1997**, *453*, 1411–1443. [CrossRef]

22. Wang, Q.; Chen, Y.; Zhang, H. A new Riccati equation rational expansion method and its application to (2+ 1)-dimensional Burgers equation. *Chaos Solitons Fractals* **2005**, *25*, 1019–1028. [CrossRef]

23. Ozisik, M.; Secer, A.; Bayram, M. On solitary wave solutions for the extended nonlinear Schrödinger equation via the modified F-expansion method. *Opt. Quantum Electron.* **2023**, *55*, 215. [CrossRef]

24. Murad, M.A.S.; Hamasalh, F.K.; Ismael, H.F. Optical soliton solutions for time-fractional Fokas system in optical fiber by new Kudryashov approach. *Optik* **2023**, *280*, 170784. [CrossRef]

25. Yokus, A.; Isah, M.A. Dynamical behaviors of different wave structures to the Korteweg–de Vries equation with the Hirota bilinear technique. *Phys. A Stat. Mech. Its Appl.* **2023**, *622*, 128819. [CrossRef]

26. Liu, S.Z.; Wang, J.; Zhang, D.J. The Fokas-Lenells equations: Bilinear approach. *Stud. Appl. Math.* **2022**, *148*, 651–688. [CrossRef]

27. Rezazadeh, H.; Korkmaz, A.; Khater, M.M.; Eslami, M.; Lu, D.; Attia, R.A. New exact traveling wave solutions of biological population model via the extended rational sinh-cosh method and the modified Khater method. *Mod. Phys. Lett. B* **2019**, *33*, 1950338. [CrossRef]

28. Hereman, W.; Banerjee, P.P.; Korpel, A.; Assanto, G.; Van Immerzeele, A.; Meerpoel, A. Exact solitary wave solutions of nonlinear evolution and wave equations using a direct algebraic method. *J. Phys. Math. Gen.* **1986**, *19*, 607. [CrossRef]

29. Khater, M.M. Novel computational simulation of the propagation of pulses in optical fibers regarding the dispersion effect. *Int. J. Mod. Phys. B* **2023**, *37*, 2350083. [CrossRef]

30. Khater, M.M.; Zhang, X.; Attia, R.A. Accurate computational simulations of perturbed Chen–Lee–Liu equation. *Results Phys.* **2023**, *45*, 106227. [CrossRef]

31. Ma, W.X. Lump solutions to the Kadomtsev–Petviashvili equation. *Phys. Lett. A* **2015**, *379*, 1975–1978. [CrossRef]

32. Kumar, A.; Kumar, S. Dynamic nature of analytical soliton solutions of the (1+ 1)-dimensional Mikhailov-Novikov-Wang equation using the unified approach. *Int. J. Math. Comput. Eng.* **2023**, *1*, 217–228. [CrossRef]

33. Khater, M.M. Computational simulations of propagation of a tsunami wave across the ocean. *Chaos Solitons Fractals* **2023**, *174*, 113806. [CrossRef]

34. Wazwaz, A.M. The tanh and the sine–cosine methods for a reliable treatment of the modified equal width equation and its variants. *Commun. Nonlinear Sci. Numer. Simul.* **2006**, *11*, 148–160. [CrossRef]

35. Khater, M.M. Abundant and accurate computational wave structures of the nonlinear fractional biological population model. *Int. J. Mod. Phys. B* **2023**, *37*, 2350176. [CrossRef]

36. Younas, U.; Sulaiman, T.A.; Ren, J.; Yusuf, A. Lump interaction phenomena to the nonlinear ill-posed Boussinesq dynamical wave equation. *J. Geom. Phys.* **2022**, *178*, 104586. [CrossRef]

37. Trudinger, N.S.; Wang, X.J. The Monge-Ampère equation and its geometric applications. *Handb. Geom. Anal.* **2008**, *1*, 467–524.

38. Lou, S.Y.; Lu, J. Special solutions from the variable separation approach: The Davey-Stewartson equation. *J. Phys. A Math. Gen.* **1996**, *29*, 4209. [CrossRef]

39. Anderson, D.R.; Ulness, D.J. Properties of the Katugampola fractional derivative with potential application in quantum mechanics. *J. Math. Phys.* **2015**, *56*, 6. [CrossRef]

40. Al-Mdallal, Q.M.; Abdeljawad, T.; Hajji, M.A. Theoretical and numerical results for fractional difference and differential equations. *Discret. Dyn. Nat. Soc.* **2017**, *2017*, 2543452. [CrossRef]

41. Ortigueira, M.D.; Rodríguez-Germá, L.; Trujillo, J.J. Complex Grünwald–Letnikov, Liouville, Riemann–Liouville, and Caputo derivatives for analytic functions. *Commun. Nonlinear Sci. Numer. Simul.* **2011**, *16*, 4174–4182. [CrossRef]

42. Tachikawa, M.; Shiga, M. Evaluation of atomic integrals for hybrid Gaussian type and plane-wave basis functions via the McMurchie-Davidson recursion formula. *Phys. Rev. E* **2001**, *64*, 056706. [CrossRef] [PubMed]

43. Akram, G.; Sadaf, M.; Zainab, I. Observations of fractional effects of $\beta$-derivative and M-truncated derivative for space time fractional Phi-4 equation via two analytical techniques. *Chaos Solitons Fractals* **2022**, *154*, 111645. [CrossRef]

44. Onder, I.; Cinar, M.; Secer, A.; Bayram, M. Analytical solutions of simplified modified Camassa-Holm equation with conformable and M-truncated derivatives: A comparative study. *J. Ocean. Eng. Sci.* **2022**. [CrossRef]

45. Abdelhakim, A.A.; Machado, J.A.T. A critical analysis of the conformable derivative. *Nonlinear Dyn.* **2019**, *95*, 3063–3073. [CrossRef]

46. Yadav, S.; Pandey, R.K.; Shukla, A.K. Numerical approximations of Atangana–Baleanu Caputo derivative and its application. *Chaos Solitons Fractals* **2019**, *118*, 58–64. [CrossRef]

47. Bayrak, A.M. Application of the $(G'/G)$-expansion method for some space-time fractional partial differential equations. *Commun. Fac. Sci. Univ. Ank. Ser. Math. Stat.* **2018**, *67*, 60–67.

48. Jumarie, G. Fractional partial differential equations and modified Riemann-Liouville derivative new methods for solution. *J. Appl. Math. Comput.* **2007**, *24*, 31–48. [CrossRef]

49. Jhangeer, A.; Almusawa, H.; Rahman, R.U. Fractional derivative-based performance analysis to Caudrey-Dodd-Gibbon-Sawada-Kotera equation. *Results Phys.* **2022**, *36*, 105356. [CrossRef]
50. Baskonus, H.M.; Mahmud, A.A.; Muhamad, K.A.; Tanriverdi, T. A study on Caudrey-Dodd-Gibbon-Sawada-Kotera partial differential equation. *Math. Methods Appl. Sci.* **2022**, *45*, 8737–8753. [CrossRef]
51. Hilfer, R. Fractional diffusion based on Riemann-Liouville fractional derivatives. *J. Phys. Chem. B* **2000**, *104*, 3914–3917. [CrossRef]
52. Almeida, R. A Caputo fractional derivative of a function with respect to another function. *Commun. Nonlinear Sci. Numer. Simul.* **2017**, *44*, 460–481. [CrossRef]
53. Baleanu, D.; Inc, M.; Yusuf, A.; Aliyu, A.I. Lie symmetry analysis, exact solutions and conservation laws for the time fractional Caudrey-Dodd-Gibbon-Sawada-Kotera equation. *Commun. Nonlinear Sci. Numer. Simul.* **2018**, *59*, 222–234. [CrossRef]
54. Saha Ray, S. New soliton solutions of conformable time fractional Caudrey–Dodd–Gibbon–Sawada–Kotera equation in modeling wave phenomena. *Mod. Phys. Lett. B* **2019**, *33*, 1950202. [CrossRef]
55. Cheng, W.G.; Li, B.; Chen, Y. Bell polynomials approach applied to (2+ 1)-dimensional variable-coefficient Caudrey-Dodd-Gibbon-Kotera-Sawada equation. *Abstr. Appl. Anal.* **2014**, *2014*, 523136. [CrossRef]
56. Kumar, S.; Mohan, B.; Kumar, A. Generalized fifth-order nonlinear evolution equation for the Sawada-Kotera, Lax, and Caudrey-Dodd-Gibbon equations in plasma physics: Painlevé analysis and multi-soliton solutions. *Phys. Scr.* **2022**, *97*, 035201. [CrossRef]
57. Geng, X.; He, G.; Wu, L. Riemann theta function solutions of the Caudrey-Dodd-Gibbon-Sawada-Kotera hierarchy. *J. Geom. Phys.* **2019**, *140*, 85–103. [CrossRef]
58. Qu, Q.X.; Tian, B.; Sun, K.; Jiang, Y. Bäcklund transformation, Lax pair, and solutions for the Caudrey-Dodd-Gibbon equation. *J. Math. Phys.* 2011, *52*, 013511. [CrossRef]
59. Khan, K.; Akbar, M.A. Study of explicit travelling wave solutions of nonlinear evolution equations. *Partial. Differ. Equ. Appl. Math.* **2023**, *7*, 100475. [CrossRef]
60. Muhammad, T.; Hamoud, A.A.; Emadifar, H.; Hamasalh, F.K.; Azizi, H.; Khademi, M. Traveling wave solutions to the Boussinesq equation via Sardar sub-equation technique. *AIMS Math.* **2022**, *7*, 11134–11149.
61. Roy-Chowdhury, A.K. *Painlevé Analysis and Its Applications*; CRC Press: Boca Raton, FL, USA, 1999; Volume 105.